ACS OMEGA

Open Access

http://pubs.acs.org/journal/acsodf

Article

In Vitro Antibacterial and DPPH Radical Inhibitory Activities and *In Silico* Molecular Simulation of Compounds Isolated from the Leaves of *Olinia rochetiana*

Tolessa Duguma, Yadessa Melaku,* Daniel Rentsch, Mo Hunsen, Taye B. Demissie, and Nayang Kgakatsi

Cite This: *ACS Omega* 2025, 10, 9547−9562

Read Online

ACCESS | Metrics & More | Article Recommendations | Supporting Information

ABSTRACT: *Olinia rochetiana* is one of the medicinal plants traditionally used in Ethiopia to treat various ailments, including wounds, snake bites, tuberculosis, and cancer. However, there is a lack of comprehensive investigation regarding the biological activities of the phytoconstituents extracted from its leaves. This study aims to isolate compounds and evaluate their *in vitro* antibacterial properties and DPPH radical scavenging activities, complemented by *in silico* molecular modeling. Thirteen compounds were identified using GC−MS from combined fractions 4−17. Ursolic acid (**14**), 5-hydroxy-4-methyl-5,6-dihydro-(2*H*)-pyran-2-one (**15**), hyperoside (**16**), and 4-*O*-*β*-D-glucopyranosylcaffeic acid (**17**) were purified using chromatographic techniques and characterized using 1D and 2D NMR spectral data and a thorough comparison with literature data. At 5 mg/mL, the inhibition zones (IZs) of isolated compounds ranged from 9.00 to 12.67 mm against all of the evaluated bacteria. Among all isolated compounds, compound **14** exhibited more inhibition against *Streptococcus pyogenes* with an inhibition zone of 12.67 mm, and compound **17** also exhibited potent inhibition activity against *Staphylococcus aureus* with an inhibition zone of 11.00 mm. *Escherichia coli* and *Pseudomonas aeruginosa* were better inhibited using compound **16** with IZs of 12.30 and 11.70 mm, respectively. The antibacterial activity of compound **16** against *E. coli* and *P. aeruginosa*was validated using *in silico* molecular docking studies against the target enzymes *E. coli* DNA gyrase B (−8.4 kcal/mol) and *Pseudomonas* quinolone signal A (−9.3 kcal/mol), respectively. At 62.5 *μ*g/mL, the highest (89.2%) and the lowest (50.5%) DPPH radicals were scavenged by compounds **16** and **14**, respectively. Compounds **14**, **15**, and **17** obey Lipinski's rule of five, and none of the isolated compounds were predicted to be fatal if swallowed. These findings reinforce the traditional use of the plant as a remedy for various bacterial diseases. However, further *in vivo* studies are essential to assess the biological and toxicological properties of the isolated compounds.

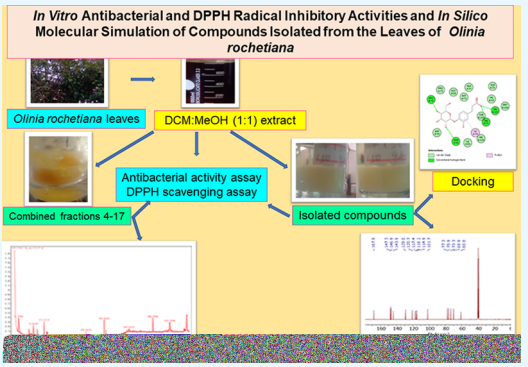

1. INTRODUCTION

Olinia rochetiana A. Juss (Figure 1) is a notable traditional medicinal plant in Ethiopia, belonging to the genus *Olinia* within the family Penaeaceae.[1] Locally known as *Nole* in Afan Oromo, this species is native to Ethiopia as well as parts of Kenya, Sudan, Tanzania, and Uganda. It grows to heights of 4 to 27 m. Traditionally, the leaves of the plant are used in Ethiopia to treat various diseases including the common cold, eczema and warts, toothache, bone tuberculosis, and wounds.[2−7] The latex is used to treat snakebite, and the root, leaf, or bark is used for the treatment of diarrheal related diseases, the evil eye, and cancer.[8−10]

The antibacterial activities of various solvent extracts from the barks and leaves of *Olinia rochetiana* have been documented.[11−15] Notably, the methanol extract from the leaves has demonstrated antidiarrheal properties.[16] Preliminary phytochemical screening of the different solvent extracts from the leaves and stem bark revealed the presence of phenols, tannins, steroids, terpenoids, saponins, and glycosides.[15] Furthermore, a compound known as cyanogenic glucoside prunasin was identified and quantified in the aqueous phase of the acetone extract from the leaves and stems of the plant.[17] However, there is a lack of detailed studies on the biological activities of the phytoconstituents extracted from the leaves of the plant. Therefore, this study aimed to isolate phytochemicals from the leaves of *O. rochetiana*and analyze their *in vitro* antibacterial and 2,2-diphenyl-1-picrylhydrazyl (DPPH) radical scavenging properties. Hence, we report here on the phytochemical constituents isolated from the leaves of the plant and their *in vitro* antibacterial and DPPH radical

Received: November 27, 2024
Revised: February 5, 2025
Accepted: February 12, 2025
Published: February 27, 2025

Figure 1. *O. rochetiana* (photo taken by Tolessa Duguma on July 12, 2021, around Cure, Waldoro Village, Homa Kebele, Abbay Chomman Woreda, Horro Guduru Zone, Oromia Region, Ethiopia).

scavenging activities. In addition, to validate the experimental antibacterial activities and predict the anticancer properties of the isolated compounds, we performed *in silico* studies of molecular docking, drug-likeness, and toxicity.

2. MATERIALS AND METHODS

2.1. Plant Materials. The leaves of *O. rochetiana* were collected in July 2021 from Waldoro village, Homa Kebele (GPS coordinates: 9°44′08.9″N, 37°16′06.2″E), Abbay Chomman Woreda, Horo Guduru Zone, Oromia region, which is approximately 300 km west of the capital, Addis Ababa, Ethiopia. The plant was identified with the help of the available literature and authenticated (TD04/2021) by Mr. Melaku Wendaferash at the National Herbarium, Biology Department, and Addis Ababa University, Ethiopia. Then, the collected plant material was immediately brought to the Organic Chemistry laboratory of Adama Science and Technology University and allowed to dry at room temperature while shaded. The dried plant material was then pulverized using an electric grinder and stored at 4 °C for further analysis.

2.2. Extraction and Isolation. The pulverized leaves of *O. rochetiana* (600 g) were extracted using DCM/MeOH (1:1, 3 L, 1 g in 5 mL) on maceration for 72 h. After being filtered, the extracts were concentrated using a rotary evaporator at 40 °C to obtain 104 g yield. The extract (25 g) was adsorbed onto 25 g of silica gel and subjected to column chromatography using 200 g of silica gel (60−200 mesh size). The column was eluted with a gradient of *n*-hexane and EtOAc (1:0 to 0:1) and EtAC and MeOH (95:5 to 1:1). A total of 200 fractions of 100 mL each were collected. Based on their TLC profile, fractions 1−3 (13 mg), 18−25 (454 mg), and 197−200 (280 mg) were discarded. Fractions 4−6 (195 mg), 7−17 (893 mg), 26−33 (127 mg), 34−81 (679 mg), 82−97 (1.640 g), 98−113 (739 mg), 114−125 (473 mg), 126−135 (640 mg), 136−150 (2.540 g), 151−160 (2.633 g), 161−165 (729 mg), 166−180 (3.845 g), 181 (498 mg), 182−189 (2.110 g), and 190−196 (4.101 g) were combined separately and saved in preweighed vials.

Fractions 4−17 were eluted using petroleum ether/EtOAc (9:1 to 85:15) and analyzed by GC−MS. In fractions 34−81, white crystals were formed. The supernatant from these fractions was decanted, and the crystals were washed by using *n*-hexane and MeOH to obtain compound **14** (35 mg). Fractions 98−113 (739 mg), which were eluted using *n*-hexane/EtOAc (1:4), were subjected to silica gel column chromatography in isocratic mode to collect 87 fractions, each 10 mL. Among these fractions, subfractions 35−66 (175 mg) were further purified using PTLC to yield compound **15** (27 mg). Fractions 136−150 (2633 mg), which were eluted with EtOAc/MeOH (95:5), were further subjected to silica gel (about 53 g) column chromatography using the isocratic mode to collect 120 fractions of 10 mL each. Subfractions 89−94 and 95−103 formed yellow and white crystals, resulting in compounds **16** (30 mg) and **17** (50 mg), respectively. Compound **16** was further purified for antibacterial and DPPH radical scavenging activities.

2.3. GC−MS Analysis. The GC−MS method utilized in the literature was followed to examine the individual components of fractions 4−17 (1088 mg).[18] Approximately 0.5 μL of the fraction with a concentration of 200 ppm was placed in an injector of an Agilent Technology 7890B gas chromatograph that had an HP-5 column with a length of 30 m, an internal diameter of 250 μm, and a 0.25 μm thick film. The GC was connected to an Agilent Technologies 5977B mass spectrometer, which had a single quadrupole type detector with a scan ability of m/z ranging from 50 to 550 at 70 eV of the EI ionization source. The total run time was 60 min, which started at 40 °C for 5 min, was raised to a final temperature of 250 °C at a heating rate of 6 °C/min, and was continued isothermally for about 20 min. The GC injector was set to the splitless mode at 250 °C. The carrier gas, helium, was set at a flow rate of 1 mL/min. The mixture of *n*-alkanes containing C7−C30 was analyzed using the same procedure as described above for essential oil to determine the retention index (RI) of each essential component using the formula given below (eq 1).

https://doi.org/10.1021/acsomega.4c10788
ACS Omega 2025, 10, 9547−9562

$$RIx = 100n + 100\left[\frac{tx - tn}{tn + 1 - tn}\right] \quad (1)$$

where "x" is the unknown compound, "tx" is the retention time (RT) of "x", "tn" is the retention time of *n*-alkane eluted just before "x", and "tn + 1" is the retention time of *n*-alkane eluted just after "x".

The W11N17 library that was loaded onto the device was used to identify the fraction components, and the RI was compared to the RI chosen from the PubChem online database.[19] Based on the peak area, the quantities of each component were determined.

2.4. NMR Experiments. The ^{1}H and ^{13}C NMR spectra were obtained using resonance frequencies of 400.2 and 100.6 MHz, respectively, on a Bruker Avance III 400 NMR spectrometer (Bruker Biospin AG, Fällanden, Switzerland) and a JNM-ECZ 400S (JEOL, Ldt. USA). A 5 mm CryoProbe Prodigy probe equipped with a *z*-gradient with 90° pulse lengths of 11.4 μs (^{1}H) and 10.0 μs (^{13}C) was used. NMR spectra were recorded at 298 K by applying Bruker standard pulse programs and parameter sets to obtain all 1D ^{1}H and ^{13}C NMR as well as the 2D correlated NMR data ($^{1}H-^{1}H$ DQF-COSY, $^{1}H-^{13}C$ HSQC, and $^{1}H-^{13}C$ HMBC). The resonances of DMSO at δ = 2.49/39.5 ppm were used for calibrating the ^{1}H and ^{13}C NMR chemical shifts (δ) in ppm.

2.5. *In Vitro* Antibacterial Activity. The antibacterial activity evaluation was conducted using the disk diffusion method against two Gram-positive bacteria, including *S. aureus* (ATCC 25923) and *S. pyogenes* (ATCC 19615), and two Gram-negative bacteria, including *E. coli* (ATCC 25922) and *P. aeruginosa* (ATCC 27853), using the procedure reported in the literature.[20] In detail, 38 g of Mueller–Hinton agar (MHA) medium was dissolved in 1 L of distilled water, heated until completely dissolved, and then allowed to cool. Twenty milliliters of the medium was dispensed into a 100 mm Petri dish to a depth of 4 mm, allowed to be solidified at room temperature, and then stored at 4 °C. The test bacteria were suspended in sterile saline ($BaCl_2$) to adjust the turbidity to the 0.5 McFarland standard, which is equivalent to a test bacteria suspension containing 1.5×10^8 cfu/mL. Within 15 min, each inoculum was inoculated on a Petri dish containing MHA using a sterile swab. A sterile 6 mm disc made of filter paper was impregnated with 20 μL of a different concentration of DCM/MeOH (1:1) extract (100, 50, and 25 mg/mL), fractions 4–17, and each isolated compound (5, 2.5, and 1.25 mg/mL); placed on the surface of the Petri dish; and incubated at 37 °C for 24 h. The diameter of the IZs was measured, provided that inactive if less than 6 mm and active if greater than 6 mm. The extent of activity of the samples was compared with the positive control ciprofloxacin (0.5 mg/mL). All samples were analyzed in triplicate, and the data were reported in the form of mean ± standard deviation.

2.6. DPPH Radical Scavenging Activity. The antioxidant activity of the extract was evaluated using a DPPH radical scavenging assay following procedures indicated in the literature.[21] In detail, 4 mg of DPPH was dissolved in 100 mL of MeOH to obtain 40 μg/mL and stored in a dark bottle at 4 °C by covering it with aluminum foil. The DCM/MeOH (1:1) extract and isolated compounds were separately dissolved in MeOH to furnish 1000 μg/mL. Each was then serially diluted (using the half dilution method) in MeOH to give 500, 250, 125, and 62.5 μg/mL. The diluted solutions of the extract and isolated compounds (1 mL each) were mixed with 1 mL of the DPPH MeOH solution (40 μg/mL). After heating to 37 °C in the oven for 30 min, the absorbance of both the control and experimental samples was measured by using a UV–vis spectrometer at 517 nm with MeOH as a blank. The percent (%) inhibition of the DPPH free radical by the sample was calculated (eq 2). IC_{50} was calculated from a regression line.[22] Ascorbic acid was used as a standard. All samples were analyzed in triplicate, and the data were reported in the form of mean ± standard deviation.

$$\frac{A_c - A_s}{A_c} \times 100\% \quad (2)$$

where A_c is the absorbance of the control and A_s is the absorbance of the sample.

2.7. *In Silico* Molecular Docking Study of Isolated Compounds. The docking of isolated compounds with different model proteins was carried out according to the procedure described.[23] The structures of the compounds were drawn using ChemDraw 22.0 and saved in .mol file format. Subsequently, the structure was prepared for docking using the Discovery Studio Visualizer 12.1 software and saved in .pdb file format.[24] The structures of the model proteins *E. coli* DNA gyrase B (PDB ID: 7P2M), *Pseudomonas* quinolone signal A (PqsA; PDB ID: 5OE4), pyruvate kinase M2 (PKM2; PDB ID: 4G1N), and human topoisomerase IIβ (PDB ID: 3QX3) were downloaded from the Protein Data Bank and saved in .pdb file format.[25] The target proteins were cleaned using the Discovery Studio Visualizer software, and the binding sites were identified. The docking simulations were performed with AutoDock Vina and the supporting software MGLtools 1.5.6 and Python 3.10.9. Each run was carried out for nine conformers by default. The conformer with the lowest binding energy was selected and analyzed with Discovery Studio Visualizer to visualize the interactions between the ligand and target in 2D and 3D structures. For comparison, simulations were carried out for positive controls: ciprofloxacin (antibacterial agent), etoposide (anticancer drug of topoisomerase II inhibitor), and PKM2-IN-1 (anticancer agent of pyruvate kinase M2 inhibitor).

2.8. *In Silico* Pharmacokinetics and Toxicity of the Isolated Compounds. The canonical simplified molecular-input line-entry system (SMILES) of known isolated compounds was retrieved from the PubChem database and submitted to the SwissADME online tool to estimate properties such as physicochemical properties, lipophilicity, water solubility, and drug-likeness.[26] For the prediction of *in silicon* acute toxicity (the six classes of oral toxicity), organ toxicity, and toxicity end points, the SMILESs of isolated compounds were submitted to the Pro Tox 3.0 online tool.[27] The result of the isolated compounds was compared with the standard antibacterial drug ciprofloxacin and standard anticancer agents PKM2-IN-1 and etoposide.

3. RESULTS AND DISCUSSIONS

3.1. Characterization of Compounds from the Leaves of *O. rochetiana*. *3.1.1. GC–MS Composition Analysis of Combined Fractions 4–17.* From the data generated using the GC–MS analysis of fractions 4–17 of *O. rochetiana* leaves (Figure S1), 26 components were identified. Among all components, 13 (62.06%) components (Table 1) have been identified (Figure 2) by comparing their calculated retention indexes and mass fragments with the data from the PubChem database.[19]

https://doi.org/10.1021/acsomega.4c10788
ACS Omega 2025, 10, 9547–9562

Table 1. Compounds Identified from Fractions 4−17 of *O. rochetiana* Leaves Using GC−MS

S/N	compound name	RT	RI		%A
			calculated	reported	
1	4-ethynylcyclopentene	5.11	757.2		20.84
2	*meso*-2,5-dimethyl-3,4-hexanediol	10.43	923.5		0.81
3	3-methyl-5-methylene-2(5*H*)-furanone	13.31	1015.5		4.93
4	diethylbenzene	14.18	1045.7	1047	0.92
5	(*S*)-(−)-4-benzoyloxy-5-oxopentyl pivalate	15.47	1091.1		0.27
6	isooctanol	22.59	1383.8		0.16
7	(*E*)-methyl 5-(6-fluoropyridin-3-yl)-5-hydroxypent-2-enoate	26.83	1589.2		0.71
8	dibutyl phthalate	31.74	1859.6		0.22
9	methyl palmitate	32.64	1913.0	1913	2.84
10	palmitic acid	33.16	1944.5	1945	0.92
11	ditridecyl phthalate	33.30	1953.4		0.43
12	5,9,13,17-tetramethyl 4,8,12,16-octadecatetraenoic acid	48.30	2811.0		6.0
13	neophytadiene	59.18			23.0

Neophytadiene (**13**, 23.0%) was the most dominant component followed by 4-ethynylcyclopentene (**1**, 20.84%), 5,9,13,17-tetramethyl 4,8,12,16-octadecatetraenoic acid (**12**, 6.0%), 3-methyl-5-methylene-2(5*H*)-furanone (**3**, 4.93%), and methyl palmitate (**9**, 2.84%). The dominant component, neophytadiene (**13**), has been reported to have a wide range of biological activities, including anxiolytic-like, anticonvulsant, anticancer, anti-inflammatory, and antibacterial activities.[28−31] A report in the literature indicated that 4-ethynylcyclopentene (**1**) was found in Nam-Hom coconut.[32] The fractions containing 1-ethynylcyclopentene, which is close to compound **1** in the skeleton, displayed mosquito larvicidal activity.[33] An EtOH extract from *Zea mays*cob containing 1.0% of methyl palmitate (**9**), 0.6% of palmitic acid (**10**), and 0.4% of 5,9,13,17-tetramethyl 4,8,12,16-octadecatetraenoic acid (**12**) was reported to have DPPH radical scavenging activities.[34] In addition, compound **9** was reported for its anti-inflammatory activities.[35] The derivatives of 3-methyl-5-methylene-2(5*H*)-furanone (**3**) were reported for their antibacterial activity.[36] Essential oil containing about 7 and 3.4% of (*E*)-methyl 5-(6-fluoropyridin-3-yl)-5-hydroxypent-2-enoate (**7**) showed repellant activities against product insects and DPPH radical scavenging activities, respectively.[37,38] Natural-based phthalates dibutyl phthalate (**8**) and ditridecyl phthalate (**11**) were reported to have antibacterial, DPPH radical scavenging, and antidiabetic activities.[39,40] Therefore, the nonpolar extract of the leaves of *O. rochetiana*has a wide range of biological activities.

3.1.2. Characterization of Isolated Compounds. Four compounds (Figure 3), including ursolic acid (**14**), 5-hydroxy-4-methyl-5,6-dihydro-(2*H*)-pyran-2-one (**15**), hyperoside (**16**), and 4-*O*-*β*-D-glucopyranosylcaffeic acid (**17**), were isolated and characterized from the leaves of *O. rochetiana*. The assignment of 1D and 2D NMR data led to the identification of the chemical structures of the isolated compounds, as described below.

Compound **14** was isolated as a white solid with a melting point of 283−286 °C, which agrees with data reported previously for ursolic acid (identification described below).[41] The TLC showed an R_f value of 0.6 using *n*-hexane/EtOAc (7:3) as the mobile phase (Figure S30).

The NMR spectral data (Figures S2−S4) clearly indicate that the chemical structure of compound **14** is likely a terpenoid. In the ^{13}C NMR spectrum (Figure S3), 29 well-resolved carbon resonances were obtained. With the aid of a DEPT-135 NMR experiment (Figure S4), six quaternary carbons were identified. One additional signal of a quaternary carbon was detected in the 2D HMBC NMR experiment only since in the 1D ^{13}C NMR spectrum, it is hidden under the signal of the solvent DMSO. In addition, 9 methylene carbons and 14 carbons of CH or CH_3 groups were observed (full analysis of the 2D NMR data revealed that seven of both types of carbons were present, Table 2, Figures S5−S7). The resonance at δ^1H = 2.99 of a hydrogen directly connected to a carbon at δ^{13}C = 76.8 can most probably be assigned to a −CH(OH) group and was used as a starting point for the stepwise assignment of all carbon and hydrogen signals via the 2D ^{1}H−^{13}C HSQC and HMBC NMR correlations (Table 2). The crucial HMBC correlations used

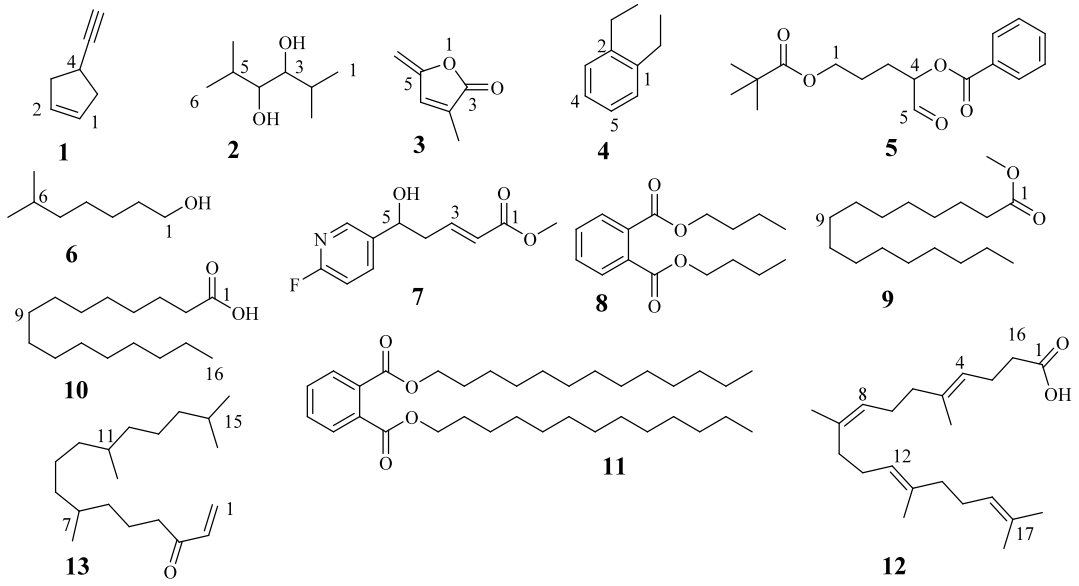

Figure 2. Structures of compounds from fractions 4−17 characterized using the GC−MS spectral data.

https://doi.org/10.1021/acsomega.4c10788
ACS Omega 2025, 10, 9547−9562

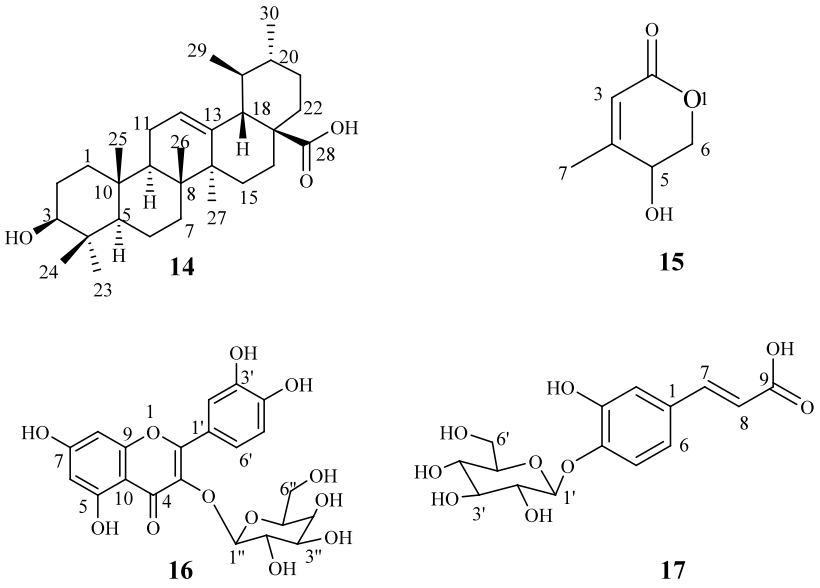

Figure 3. Chemical structures of isolated compounds characterized using NMR spectral data.

Table 2. ^{1}H NMR (400.2 MHz) and ^{13}C NMR (100.6 MHz) Spectral Data of Compound 14 and NMR Data Reported for Ursolic Acid

	compound **14**/DMSO-d_6				ursolic acid/pyridine-d_5[42]	
position	δ^{1}H	δ^{13}C	COSY	^{1}H−^{13}C HMBC	δ^{1}H	δ^{13}C
1	1.52 + 0.90 (m, 2H)	38.2			1.58 + 1.00	39.2
2	1.5−1.4 (m, 2H)	27.0	H-3	C-3	1.81	28.2
3	2.99 (m, 1H)	76.8	H-2, 3-OH	C-2, 4, 23, 24	3.44	78.2
4		38.4				39.6
5	0.65 (m, 1H)	54.8			0.88	55.9
6	1.45 + 1.29 (m, 2H)	18.0		C-5, 8	1.58 + 1.39	18.8
7	1.43 + 1.26 (m, 2H)	32.7			1.59 + 1.39	33.7
8		38.5				40.1
9	1.45 (m, 1H)	46.8			1.65	48.1
10		36.5				37.5
11	1.83 (m, 2H)	22.8	H-12		1.96	23.7
12	5.12 (t, 3.2 Hz, 1H)	124.6	H-11	C-9, 11, 14, 18	5.49	125.7
13		138.2				139.3
14		41.6				42.6
15	1.80 + 0.98 (m, 2H)	27.5		C-8, 12, 13, 16	2.33 + 1.22	28.8
16	1.92 + 1.51 (m, 2H)	23.8		C-15, 17, 28	2.14 + 2.01	25.0
17		47.0				48.1
18	2.10 (d, 11.2 Hz)	52.4	H-19	C-12, 13, 14, 16, 17, 19, 20, 28, 29	2.63	53.6
19	1.29 (m, 1H)	38.4	H-18, 29		1.49	39.5
20	0.90 (m, 1H)	38.4			1.05	39.4
21	1.41 + 1.27 (m, 2H)	30.2			1.49 + 1.40	31.1
22	1.6−1.5 (m, 2H)	36.3		C-20, 28	1.97	37.4
23	0.88 (s, 3H)	28.3	H-24	C-3, 4, 5, 24	1.24	28.8
24	0.66 (s, 3H)	16.1	H-23	C-3, 4, 5, 23	1.02	16.5
25	0.85 (s, 3H)	15.2		C-1, 5, 9, 10	0.92	15.7
26	0.74 (s, 3H)	16.9		C-7, 8, 9, 14	1.06	17.5
27	1.03 (s, 3H)	23.3		C-8, 13, 14, 15	1.24	24.0
28		178.3				179.7
29	0.80 (d, 6.3 Hz, 3H)	17.0	H-19	C-18, 19, 20	1.02	17.5
30	0.90 (br, 3H)	21.1		C-19, 20, 21	0.97	21.4
3-OH	4.28 (d, 5.1 Hz, 1H)		H-3	C-2, 3, 4		
17-COOH	11.9 (s(br), 1H)					

for establishing the chemical structure of the terpenoid skeleton are shown in Figure 4. Once the terpenoid skeleton was assigned, a comparison with literature data showed that fraction **14** could be ursolic acid.[42] Although the NMR data in the cited paper were recorded under completely different conditions (NMR solution in pyridine at 310 K) than in our experiments

https://doi.org/10.1021/acsomega.4c10788
ACS Omega 2025, 10, 9547−9562

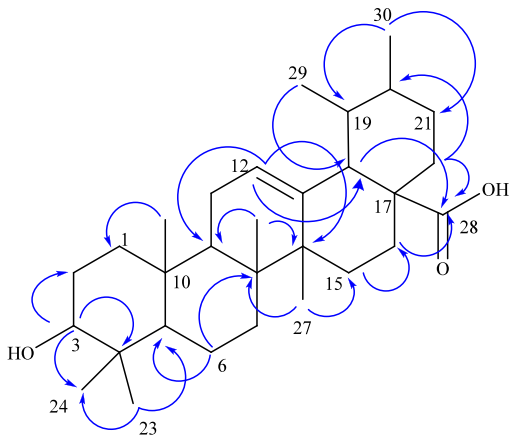

Figure 4. Crucial $^{1}H-^{13}C$ HMBC NMR correlations were identified for the assignment of the skeleton of the chemical structure of sample **14**.

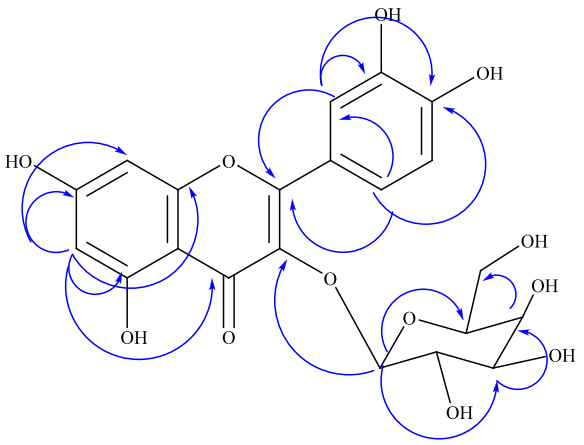

Figure 5. Crucial $^{1}H-^{13}C$ HMBC NMR correlations were identified for the assignment of the skeleton of the chemical structure of compound **16**.

(DMSO at 298 K), all ^{13}C NMR chemical shifts agree very well (deviations of the $\delta^{13}C$ NMR data of only +0.3 to +1.5 ppm, see Table 2). In all cases where the two diastereotopic protons of the methylene groups in the literature show well-distinguished ^{1}H NMR resonances, this behavior has been observed for our data as well (^{1}H NMR data at positions 1, 6, 7, 15, 16, and 21 in Table 2). As a result of the interpretation work, long-range correlations (Figure S6) of the methyl protons (positions 6 and 27) to a ^{13}C resonance at 39.1 (position 8) were observed. This is exactly the resonance of a quaternary carbon that was missing in the 1D ^{13}C NMR data. Ursolic acid (**14**) is known for its wide range of biological activities. It has been reported to exhibit antibacterial, antioxidant, anticancer, antidiabetic, anti-inflammatory, and antiviral activities.[43−46]

Compound **15** was isolated as a brown, amorphous solid. TLC showed a spot at an R_f value of 0.4 by using *n*-hexane/EtOAc (3:2) (Figure S30). In the ^{1}H NMR spectrum (Figure S8), resonances of two single methine protons were observed at 5.91 and 4.96 ppm (both are multiplets), and the signal of a methyl group is found at δ 2.03 (dd, J = 1.5 and 0.4 Hz). Further, partly hidden in the foot of the water resonance, two possibly diastereotopic protons both appearing with doublet × doublet coupling patterns at 3.77 and 3.62 ppm were observed. In the ^{13}C NMR data, in total, six carbons have been identified (Figures S9 and S10): two methine C's at 116.7 and 85.2 ppm, one methylene (59.4 ppm), one methyl (13.6 ppm), and two quaternary C's at 173.1 and 168.1 ppm. The chemical structure of compound **15** was established over the analysis of the 2D NMR spectral data (Figures S11 to S13). From $^{1}H-^{13}C$ long-range correlations detected from the methyl protons at 2.03 ppm to four carbons, the ^{1}H and ^{13}C NMR spin system at positions 2−5 of compound **15** was assignable, and the chemical structure was finally identified as 5-hydroxy-4-methyl-5,6-dihydro-(2*H*)-pyran-2-one. All NMR data are summarized in Table 2 and compared with the NMR data of this residue esterified at position 5 to caffeic acid.[47]

Compound **16** was isolated as a yellow solid with a melting point of 243−246 °C, which is in agreement with the data reported for hyperoside (discussion of NMR data, see below).[48] The TLC showed a spot at R_f value 0.7 using EtOAc/MeOH (24:1) as the mobile phase (Figure S30). Based on the ^{1}H NMR spectral data (with $\delta^{1}H$ at 7.65, 7.51, and 6.80 ppm, as shown in Figure S14) and DQF-COSY correlations (Figure S17, relevant J_{HH} of 8.5 and 2.1 Hz), compound **16** was found to possess a spin system characteristic of a 1,2,4-substituted aromatic moiety. The carbons at positions 1' to 6' (as depicted in Figure 3) were assigned using one-bond (^{1}J) and multibond $^{1}H-^{13}C$ NMR correlations. The aromatic ring must be connected through correlations from H-2' and H-6' to an exocyclic carbon C-2 at 156.2 ppm (Table 3), which was ultimately identified as part of a 4H-chromen-4-one structure. Two additional ^{1}H NMR resonances observed at 6.39 and 6.18 ppm (J_{HH} = 1.9 Hz) were identified as being in *meta* positions to each other within a 1,2,4,6-tetrasubstituted second aromatic system. Long-range correlations from the two aforementioned ^{1}H NMR signals indicated connections to a total of five different quaternary carbons, as well as to each other due to their *meta* positions. The correlation of both protons to a carbon at 177.4 ppm suggested that a carbonyl group is directly attached to the tetrasubstituted

Table 3. ^{1}H NMR (400.2 MHz) and ^{13}C NMR (100.6 MHz) Spectral Data of Compound 15 and NMR Data Reported in the Literature[47]

	compound **15**/DMSO-d_6				5-hydroxy-4-methyl-5,6-dihydro-(2*H*)-pyran-2-one residue[47]	
no.	$\delta^{1}H$ (J in Hz)	$\delta^{13}C$	COSY	$^{1}H-^{13}C$ HMBC	$\delta^{1}H$	$\delta^{13}C$/MeOD
2		173.1				173.9
3	5.91 (m, 1H)	116.7	H-5, 7	C-2, 4, 5, 7	5.98 (t, J = 1.5, 1H)	117.4
4		168.1				167.5
5	4.96 (m, 1H)	85.2	H-3, 6	C-3, 4, 6	5.26 (m, 1H)	83.1
6	3.77 (dd, J = 2.9, 12.5, 1H) 3.62 (dd, J = 3.6, 12.5, 1H)	59.4	H-5	C-4, 5	4.48 (dd, J = 4.0, 12.4, 1H) 4.61 (dd, J = 3.2, 12.4, 1H)	60.1
7	2.03 (dd, J = 0.4, 1.5, 3H)	13.6	H-3, 5	C-2, 3, 4, 5	2.17 (dd, J = 0.8, 1.6, 3H)	12.5

https://doi.org/10.1021/acsomega.4c10788
ACS Omega 2025, 10, 9547−9562

Table 4. ^{1}H NMR (400.2 MHz) and ^{13}C NMR (100.6 MHz) Spectral Data of Compound 16 and NMR Data Reported for Quercetin-3-*O*-(1-D-galactopyranoside)

	compound **16**, DMSO-d_6				hyperoside[48]
C-No	δ^1H	δ^{13}C	COSY	^{1}H−^{13}C HMBC	δ^{13}C, DMSO-d_6
1					
2		156.2			156.2
3		133.5			133.5
4		177.4			177.5
5		161.2			161.2
6	6.19 (d, J = 1.9, 1H)	98.7	H-8	C-4, 5, 7, 8, 10	98.7
7		164.4			164.2
8	6.39 (d, J = 1.9, 1H)	93.5	H-6	C-4, 6, 7, 9, 10	93.5
9		156.3			156.3
10		103.8			103.8
1′		121.1			121.1
2′	7.52 (d, J = 2.1, 1H)	115.9	H-5′	C-2, 1′, 3′, 4′, 6′	115.9
3′		144.9			144.8
4′		148.5			148.5
5′	6.80 (d, J = 8.5, 1H)	115.2	H-6′	C-2(w), 1′, 2′, 3′, 4′	115.2
6′	7.65 (dd, J = 8.5, 2.1, 1H)	122.0	H-2′, 5′	C-2, 2′, 4′	122.0
1″	5.36 (d, J = 7.7, 1H)	101.8	H-2″	C-3, 2″, 3″, 5″	101.8
2″	3.56 (m, 1H)	71.2	H-1″, 3″	C-1″, 3″	71.2
3″	3.36 (m, 1H)	73.2	H-2″, 4″		73.2
4″	3.63 (m, 1H)	67.9	H-3″	C-2″, 3″, 6″	67.9
5″	3.30 (m, 1H)	75.8		C-1″	75.9
6″	3.45 and 3.29 (m, 2H)	60.1		C-5″	60.1
5-OH	12.62 (s, 1H)				

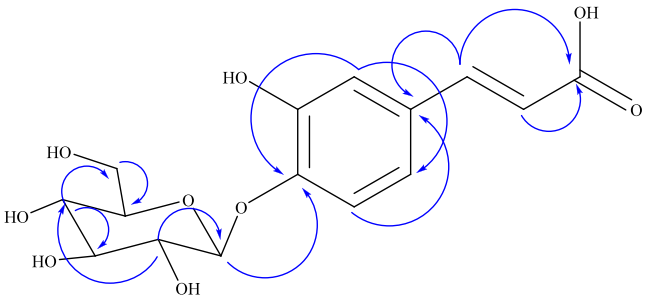

Figure 6. Crucial ^{1}H−^{13}C HMBC NMR correlations were identified for the assignment of the skeleton of the chemical structure of compound **17**.

aromatic system. As a further part of compound **16**, the ^{1}H and ^{13}C NMR spin system of a carbohydrate was identified by using the set of 2D NMR correlations. This carbohydrate moiety was linked to the 4H-chromen-4-one structure through an HMBC correlation from H1″ to C3 (Table 3, Figure S18). A literature search indicated that compound **16** must be hyperoside (Figure 5), which is a derivative of quercetin with galactose.[48] We found that the ^{13}C NMR chemical shifts reported closely match our data with deviations of only ±0.2 ppm (Table 3). Compound **17** was identified as a major impurity, as indicated by identical cross

Table 5. ^{1}H and ^{13}C NMR Chemical Shift Assignments (in) of Compound 17 and Data Reported for 4-*O*-*β*-D-Glucopyranosylcaffeic Acid

	compound **17**/DMSO-d_6				4-*O*-*β*-D-glucopyranosylcaffeic acid[49]
C-No	δ^1H	δ^{13}C	COSY	^{1}H−^{13}C HMBC	δ^{13}C/CD_3OD
1		129.0			131.2
2	7.12 (m, 1H)	114.9		C-4, 6, 7	115.7
3		146.9			148.5
4		147.3			148.7
5	7.10 (m, 1H)	116.2		C-1, 3	117.9
6	7.05 (dd, J = 8.5, 1.7, 1H)	120.7		C-2, 4, 7	122.1
7	7.45 (d, J = 15.9, 1H)	143.9	H-8	C-1, 9	146.0
8	6.31 (d, J = 15.9, 1H)	117.4	H-7	C-1, 9	118.2
9		167.9			170.6
1′	4.76 (d, J = 7.3)	101.7	H-2′	C-4	103.5
2′	3.29 (m, 1H)	73.3	H-1′	C-1′, 4′	74.8
3′	3.28 (m, 1H)	75.9	H-4′	C-1′, 2′	77.5
4′	3.17 (m, 1H)	69.9	H-3′, 5′	C-3′, 6′	71.3
5′	3.35 (m, 1H)	77.3	H-4′, 6′	C-4′, 6′	78.4
6′	3.71 (dd, J = 11.8 1.9, 1H) 3.47 (dd, J = 11.8, 5.9, 1H)	60.8	H-5′	C-4′, 5′	62.4

peaks observed in the 2D NMR spectra for both the impurity of compound **16** and compound **17**. Additionally, we have evidence for small amounts of a compound known as olinioside that consists of compound **17** esterified at C-9 with the hydroxyl group of compound **15** at position 5 (data not shown).[49] Hyperoside (**16**) is known for its numerous benefits and has been documented to exhibit a range of biological activities. It has been reported to possess antioxidant, antibacterial, anticancer, antidiabetic, anti-inflammatory, and antifungal properties).[50−55]

Compound **17** was isolated as a white solid with a melting point of 110−112 °C in accordance with the literature value of 4-*O*-*β*-D-glucopyranosylcaffeic acid (assignment of NMR data, see below).[49] The TLC displayed an R_f value of 0.6 by using EtOAc/MeOH (24:1) as the mobile phase (Figure S30). Based on the ^{13}C NMR spectral data (Table 4, Figures S21 and S22), we identified 15 carbons: 4 quaternary carbons (Cq), 10 methine carbons (CH), and 1 methylene carbon (CH_2). The chemical shifts suggest that six of these carbons are part of a carbohydrate moiety. The two protons at 7.45 and 6.31 ppm in the ^{1}H NMR spectrum (Figure S20) show a coupling constant J = 15.9 Hz, which is characteristic of an olefinic group in the E configuration. The ^{1}H−^{13}C HMBC spectrum (Figure S24 and Figure 6) shows cross-peaks at δ 7.45/129.0 and 7.45/167.9, confirming the linkage of this olefinic group to both a carboxylic carbon and an aromatic moiety. Additionally, for the second olefinic proton at 6.31 ppm, in addition to the cross-peaks mentioned above, correlations to two aromatic CH carbons at 120.7 and 114.9 ppm are observed. Although the typical coupling pattern of a 1,2,4-substituted aromatic system was not clearly observable in the ^{1}H NMR spectrum due to the similar chemical shifts (δ 7.05−7.12 ppm) of the three involved protons, leading to a higher-order spectrum, we were able to identify all resonances of positions 1−9 of compound **17** to the

https://doi.org/10.1021/acsomega.4c10788
ACS Omega 2025, 10, 9547−9562

Table 6. Antimicrobial Activity of Test Samples against Four Bacteria by Using the Disk Diffusion Method[a]

test sample	concentration (mg/mL)	IZ (mm)			
		S. aureus	*S. pyogenes*	*E. coli*	*P. aeruginosa*
DCM/MeOH (1:1) extract	100	14.93 ± 0.25	14.10 ± 0.70	14.20 ± 0.59	13.53 ± 0.37
	50	10.40 ± 0.43	9.20 ± 0.51	9.1 ± 0.37	9.5 ± 0.41
	25	7.80 ± 0.22	8.10 ± 0.17	7.60 ± 0.49	7.60 ± 0.26
fractions 4−17	5	13.8 ± 0.51	13.17 ± 0.63	13.07 ± 0.41	12.70 ± 0.59
	2,5	9.33 ± 0.47	8.43 ± 0.52	8.90 ± 0.65	9.07 ± 0.33
	1.25	NI	NI	NI	NI
14	5	10.30 ± 0.50	12.67 ± 0.27	11.53 ± 0.45	10.43 ± 0.39
	2,5	8.47 ± 0.73	10.3 ± 0.36	9.37 ± 0.55	8.47 ± 0.33
	1.25	NI	7.7 ± 0.30	NI	NI
15	5	9.20 ± 0.41	9.00 ± 0.45	9.50 ± 0.41	10.00 ± 0.39
	2,5	7.30 ± 0.42	7.07 ± 0.57	7.4 ± 0.33	7.5 ± 0.37
	1.25	NI	NI	NI	NI
16	5	10.00 ± 0.5	10.53 ± 0.46	12.30 ± 0.50	11.70 ± 0.24
	2,5	8.10 ± 0.51	8.40 ± 0.45	9.37 ± 0.46	7.77 ± 0.26
	1.25	NI	NI	NI	NI
17	5	11.00 ± 0.41	9.9 ± 0.45	9.47 ± 0.41	9.53.18 ± 0.39
	2,5	9.07 ± 0.42	7.7 ± 0.57	7.4 ± 0.33	7.5 ± 0.37
	1.25	NI	NI	NI	NI
ciprofloxacin	0.5	18.42 ± 0.26	19.93 ± 0.21	20.00 ± 0.21	22.18 ± 0.22

[a]Note: NI= no inhibition.

Table 7. DPPH Radical Scavenging Activities of the Extracts and Isolated Compounds

sample	% DPPH inhibited by each concentration in μg/mL					IC_{50} value (μg/mL)
	1000	500	250	125	62.5	
ascorbic acid	97.9 ± 0.06	97.3 ± 0.05	97.2 ± 0.05	97 0.0 ± 0.1	96.9 ± 0.06	0.5
DCM/MeOH (1:1) extract	88.33 ± 0.11	87.00 ± 0.23	82.81 ± 0.09	74.68 ± 0.15	70.60 ± 0.04	19.0
fractions 4−17	61.32 ± 0.11	57.06 ± 0.28	56.42 ± 0.04	53.37 ± 0.11	51.41 ± 0.07	11.5
14	60.41 ± 0.11	56.39 ± 0.07	55.51 ± 0.04	54.28 ± 0.11	50.50 ± 0.07	11.1
15	69.48 ± 0.14	65.46 ± 0.20	64.58 ± 0.09	63.34 ± 0.21	59.56 ± 0.13	9.4
16	96.43 ± 0.09	96.22 ± 0.15	94.62 ± 0.11	91.34 ± 0.04	89.21 ± 0.20	5.8
17	90.66 ± 0.20	89.70 ± 0.19	83.89 ± 0.23	79.24 ± 0.22	60.80 ± 0.04	31.5

Table 8. Molecular Docking Results of Isolated Compounds against *E. coli* DNA Gyrase B and PqsA (BA Is the Binding Affinity in kcal/mol)

target	ligand	BA	H-bonding	hydrophobic and electrostatic	van der Waals
E. coli DNA gyrase B	**14**	−8.1		alkyl: Ile-78	Ala-73, Asp-49, 73, Arg-76, Glu-50, Asn-46, Thr-165, Val-120, Pro-79, Ile-94
	15	−5.1	Gly-77, Thr-165	carbon hydrogen bond: Glu-50; alkyl: Ile-78	Asn-46, Asp-73, Gly-164, 75, Arg-76, Pro-79
	16	−8.4	Val-43, Met-95	carbon hydrogen bond: Val-43; Pi-cation and anion: Arg-76, Glu-50; Pi-alkyl: Pro-79, Ile-78	Arg-136, Asp-73, 49, Ala-47, Val-71, 167, 120, Thr-165, Asn-46, Ile-94, Gly-119
	17	−7.1	Arg-76	carbon hydrogen bond: Asp-73; halogen: Asp-73; amide pi-stacked: Gly-77; alkyl and pi-alkyl: Pro-79, Ile-94, Ile-78	Arg-136, Glu-50, Thr-165, Val-120, 167, 43, Asn-46, Ala-47
	ciprofloxacin	−7.4	Arg-76	carbon hydrogen bond: Asp-73; halogen: Asp-73; amide pi-stacked: Gly-77; alkyl and pi-alkyl: Pro-79, Ile-94, Ile-78	Glu-50, Thr-165, Val-120, 167, 43, Asn-46, Ala-47
PqsA	**14**	−8.2		carbon hydrogen bond: Gly-279	Ser-280, Pro-234, 205, Ile-204, Lys-206, Phe-209, Val-254
	15	−6.3	Thr-304	carbon and pi-donor hydrogen bond: Gly-307, His-308	Val-309, Gly-302, 279, 210, Ala-278, 303, Tyr-211
	16	−9.3	Thr-304, 304, Arg-397, Asp-382, 382	carbon and pi-donor hydrogen bond: Tyr-380, Gly-279, Tyr-211; Pi-alkyl: Ala-278	Val-309, Gly-302, 210, Ala-303, Ile-301, Tyr-378, Arg-372, Thr-164, His-394,
	17	−7.4	Thr-304, Tyr-378, Thr-323, Asp-382	carbon hydrogen bond: Glu-305; Pi-anion: Asp-382; amide pi-stacked: Gly-279; Pi-alkyl: Ile-301	Thr-164, Ala-303, Gly-302, 300, Pro-281, Phe-384, Asp-299, His-394, Ser-280, Arg-397
	ciprofloxacin	−7.1	Arg-397, Gly-302, Asp-299	carbon hydrogen bond: Gly-300, Thr-323; halogen: Gly-302; Pi-cation and anion: Arg-397, Asp-382; amide pi-stacked: Gly-279; alkyl and Pi-alkyl: Ile-301, His-394, Arg-397	Ala-278, Leu-282, Phe-384, Pro-281, Ser-280

https://doi.org/10.1021/acsomega.4c10788
ACS Omega 2025, 10, 9547−9562

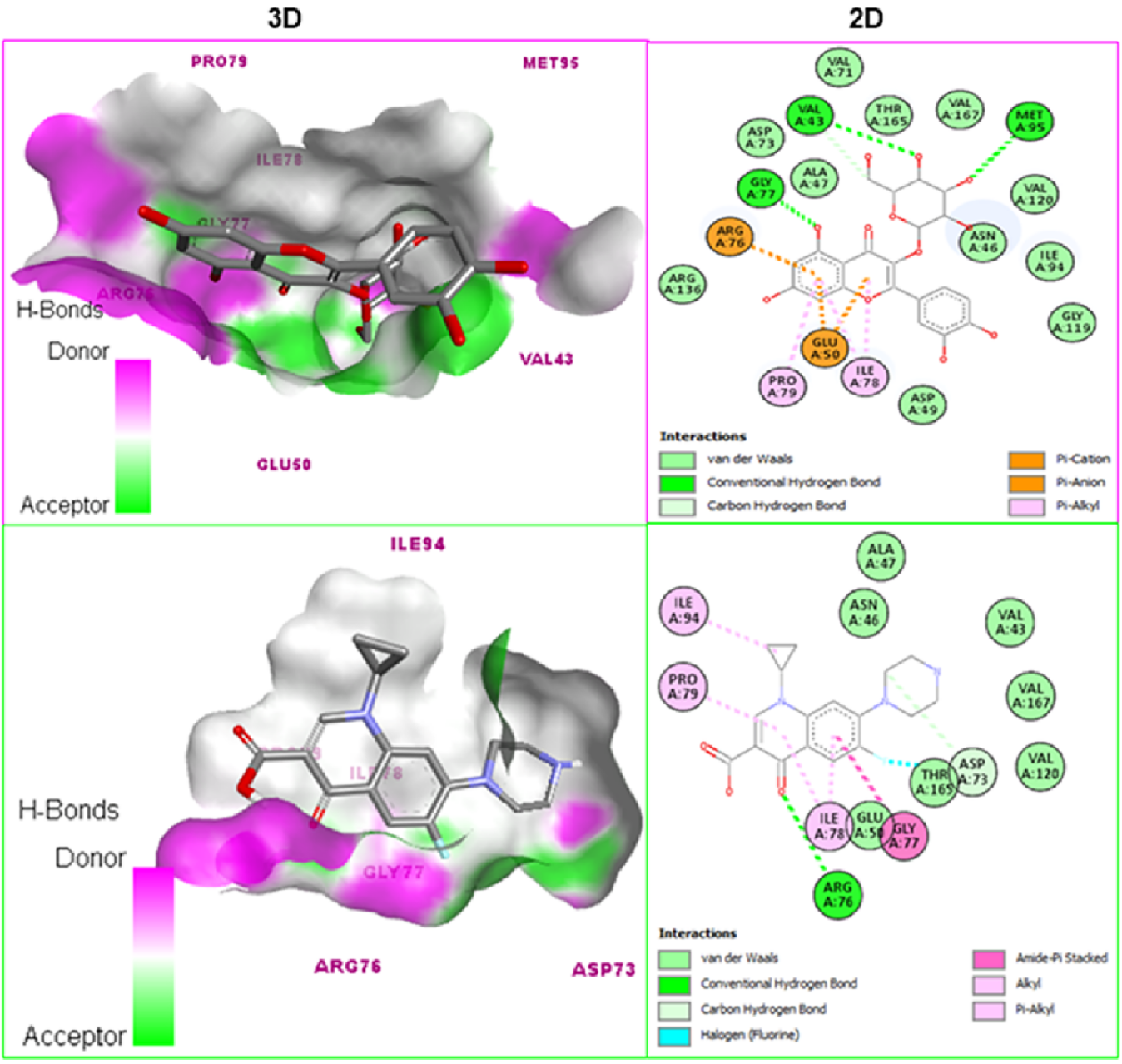

Figure 7. 3D and 2D binding interactions of compound **16** (top) and ciprofloxacin (bottom) against *E. coli* DNA gyrase.

caffeic acid moiety (Figure 3) using 2D $^{1}H-^{13}C$ NMR experiments. By analyzing the 2D NMR data, positions 1' to 6' of the carbohydrate ligand were assigned. The connection between position 1' of the carbohydrate ligand and C-4 of the caffeic acid moiety was confirmed by a cross-peak at 4.76/147.3 ppm in the HMBC NMR spectrum (Figure S24). The coupling constant of 7.3 Hz observed for H-1' indicates that the sugar moiety is present as the β-anomer. The complete NMR assignments for compound **17**, as summarized in Table 5, are compared with the data reported for 4-*O*-β-D-glucopyranosyl-caffeic acid.[49] While the reported data (spectra recorded in CD_3OD) were primarily assigned based on chemical shift arguments rather than 2D NMR correlations, our ^{13}C NMR data (recorded in DMSO) show acceptable deviations of −0.8 to −2.7 ppm compared to the published values. All relevant 2D NMR correlation signals were observed and unambiguously assigned in our analysis. 4-*O*-β-D-Glucopyranosylcaffeic acid (**17**) is reported to exhibit antibacterial and antioxidant activities.[56,57]

3.2. Antibacterial Activity. Table 6 shows the results of the antibacterial activities of extracts, fractions, and isolated compounds conducted against *S. aureus*, *S. pyogenes*, *E. coli*, and *P. aeruginosa*. The IZs of the extract (100 mg/mL) and fractions and isolated compounds (5 mg/mL) against all selected bacteria ranged from 9.00 ± 0.45 to 14.93 ± 0.25 mm, compared to the IZs of the standard antibacterial drug ciprofloxacin, which ranged from 18.42 ± 0.26 to 22.18 ± 0.22 mm. Among all selected bacteria, both DCM/MeOH (1:1, 100 mg/mL) extract and fractions 4−17 (5 mg/mL) showed the maximum IZs of 14.93 ± 0.25 and 13.8 ± 0.51, respectively, against *S. aureus*, whereas 5 mg/mL of compounds **14**, **15**, **16**, and **17** exhibited the maximum IZs of 12.67 ± 0.27, 10.00 ± 0.39, 12.30 ± 0.50, and 11.00 ± 0.41 against *S. pyogenes*, *P. aeruginosa*, *E. coli*, and *S. aureus*, respectively. Among all isolated

https://doi.org/10.1021/acsomega.4c10788
ACS Omega 2025, 10, 9547−9562

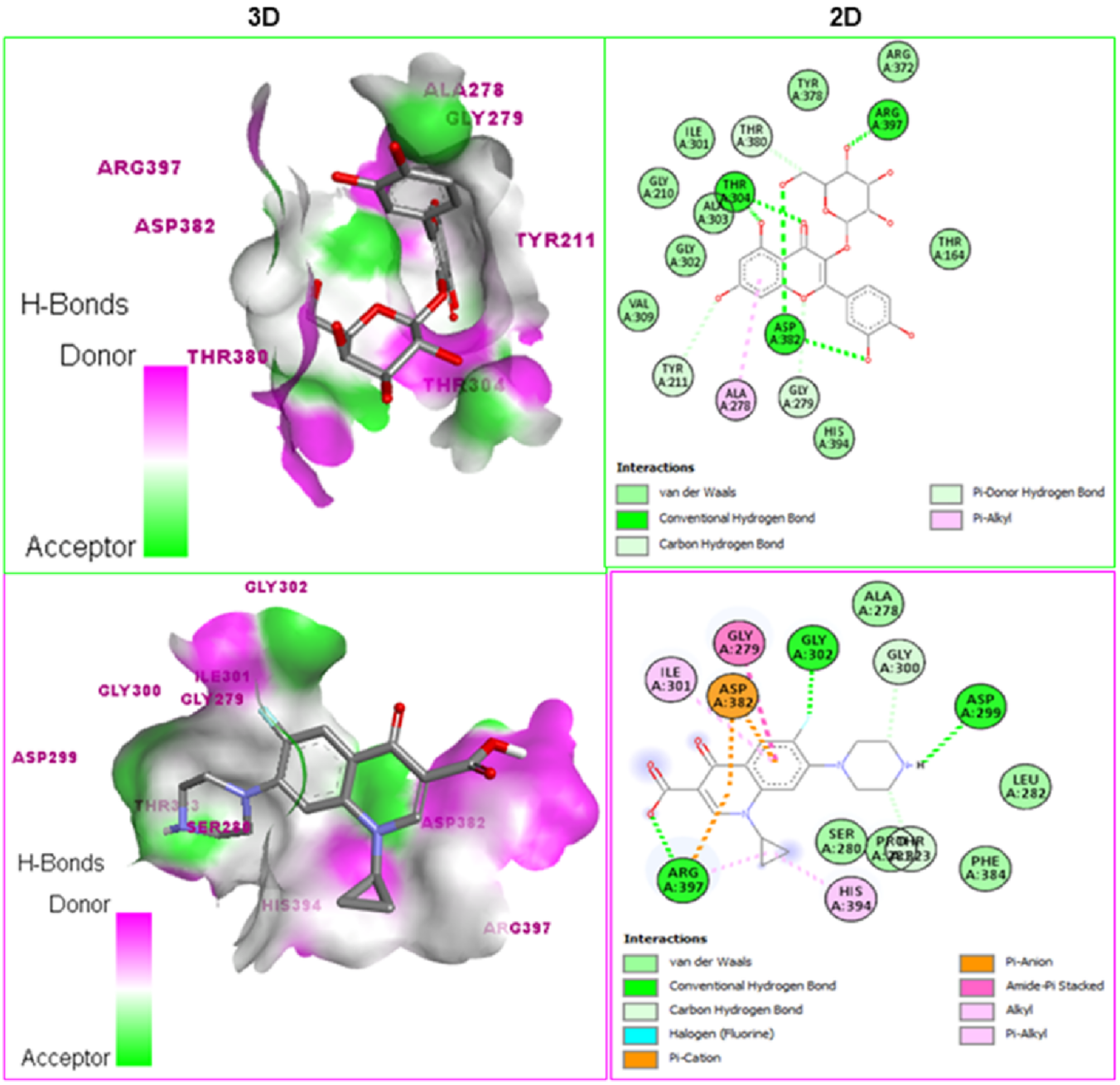

Figure 8. 3D and 2D binding interactions of compound **16** (top) and ciprofloxacin (bottom) against PqsA.

compounds, we found that *S. aureus*, *S. pyogenes*, and both *E. coli*and *P. aeruginosa*were most inhibited by compounds **17**, **14,** and **16**, respectively. However, as depicted in Table 6, the antibacterial activities of isolated compounds are less than the activities of the DCM/MeOH (1:1) extract. Some compounds in small amounts that NMR was unable to detect were observed in the extract. Therefore, we can infer that the extract may contain more active compounds in small amounts or a synergistic effect. The report in the literature indicated that our results are comparable to the results of the antibacterial activity test conducted on the various solvent extracts from the leaves of *O. rochetiana*.[12,13]

3.3. DPPH Radical Scavenging Activity. The radical scavenging ability of the extract and isolated compounds was evaluated using the DPPH assay, and the results are presented in Table 7. As indicated, at a concentration of 62.5 μg/mL, the radical scavenging abilities of the DCM/MeOH (1:1) extract and fractions 4−17 of *O. rochetiana* leaves were 70.60 and 51.41%, respectively. Compounds **14**, **15**, **16**, and **17** inhibited 50.50, 59.56, 89.21, and 60.80% DPPH radicals, respectively. The concentrations that inhibited 50% (IC_{50}) of DPPH radical were 19.0, 11.5, 11.1, 9.4, 5.8, and 31.5 μg/mL for DCM/MeOH (1:1) extract, fractions 4−17, and compounds **14**, **15**, **16**, and **17**, respectively. In comparison to the radical scavenging ability (96.9%) and the IC_{50} value (0.5 μg/mL) of the standard (ascorbic acid), compound **16** exhibited a greater radical scavenging activity than did the crude extracts and the other isolated compounds. This could be related to the number of phenolic hydroxyl groups found in compound **16**, suggesting that phenolic compounds exhibit strong antioxidant activities.[58]

3.4. *In Silico* Molecular Docking Analysis of the Isolated Compounds. The molecular docking study of

https://doi.org/10.1021/acsomega.4c10788
ACS Omega 2025, 10, 9547−9562

Table 9. Molecular Docking Results of Isolated Compounds against PKM2 and Human Topoisomerase IIβ

target	ligand	binding affinity (kcal/mol)	H-bonding	hydrophobic and electrostatic	van der Waals
PKM2	**14**	−4.1	Asp-354, Asn-350	carbon hydrogen bond: Leu-394; Pi-sigma: Phe-26; alkyl: Leu-27	Lys-311, Asn-350, Lys-311, Asp-354, Gly-355, Arg-445, Asn-318, Gln-393, Glu-397, Met-30, Phe-26, Leu-353
	15	−5.5	Tyr-390	alkyl and Pi-alkyl: Leu-394, Tyr-390, Phe-26	Leu-353, 27, Ile-389, Gln-393, Phe-26, Met-30,
	16	−9.6	Lys-311, 311, Gly-315, Asp-354, Tyr-390, Leu-394	carbon hydrogen bond: Leu-353, Ile-359; Pi-sigma: Met-30, Phe-26; Pi-pi stacked and T-shaped: Phe-26, Phe-26; Pi-sulfur: Met-30; Pi-lone pair: Asp-354	Ile-314, Leu-27, Ala-388, Glyn-393, Leu-353, Asn-350
	17	−8.5	Tyr-390, His-29, Ala-388, Tyr-390, Asp-354, Lys-311	carbon hydrogen bond: Leu-353; Pi-pi T-shaped: Phe-26	Ile-389, Leu-394, Phe-26, Leu-394, Ile-389, Leu-353, Met-90, Leu-394,
	PKM2-IN-1	−9.6	Lys-311	Pi-sigma: Leu-353; Pi-sulfur: Phe-26; Pi-pi T-shaped: Phe-26; alkyl and Pi-alkyl: Leu-353, 353, Phe-26	Asp-354, 354, Lys-311, Tyr-390, 390, Ala-388, 388, Ile-389, 389, Met-30, His-29,
human topoisomerase IIβ	**14**	−5.0			Asp-439, Arg-503, Gly-504, Lys-505, Ala-779
	15	−2.7	Arg-503	alkyl: 503	
	16	−5.1	Met-782, Gln-778, Gly-776	carbon hydrogen bond: Gly-776; Pi-sulfur: Met-782; Pi-alkyl: Arg-503, Ala-779	Lys-505, Gly-504, His-775
	17	−4.2	Gly-776, Gln-778, Arg-503	carbon hydrogen bond: Gln-778	His-775, Ala-779, Gly-504
	etoposide	−5.3	Arg-503, Gln-778	alkyl and Pi-alkyl: Ala-779	Gly-776

isolated compounds was carried out against *E. coli* DNA gyrase B, PqsA, PKM2, and human topoisomerase IIβ. *E. coli* DNA gyrase B is a bacterial enzyme responsible for DNA replication, transcription, and recombination, whereas *Pseudomonas* quinolone signal A (PqsA) is a bacterial enzyme that plays a role in the virulence factor of *P. aeruginosa*.[59,60] Pyruvate kinase M2 (PKM2) is one of the isoforms of the pyruvate kinase enzyme used to meet the energy demand for cancer cells, and human topoisomerase IIβ is a tumor cell enzyme used in the multiplication of DNA.[61−63] The results of docking analysis against *E. coli* DNA gyrase B and PqsA were compared with the standard antimicrobial ciprofloxacin (Table 8). The docking study against *E. coli* DNA gyrase B revealed that the binding affinity of the isolated compounds ranged from −8.4 to −5.1 kcal/mol compared to the binding affinity of ciprofloxacin (−7.4 kcal/mol). The highest binding score was observed with compound **16** (−8.4 kcal/mol), while the lowest binding score was observed with compound **15** (−5.1 kcal/mol). As indicated, like ciprofloxacin, compound **17** interacted with *E. coli* DNA gyrase B through only one hydrogen bond with Arg-76 amino acid residues. In contrast, compounds **15** and **16** interacted with *E. coli* DNA gyrase B was through two hydrogen bonds. However, no hydrogen bonding was observed between compound **14** and the target enzyme, *E. coli* DNA gyrase B. Compound **16** with the maximum binding affinity (−8.4 kcal/mol) exhibited good antibacterial activity against *E. coli*with an IZ of 12.30 ± 0.50 mm (Table 6). Hence, the mechanism of action of compound **16** was predicted and illustrated in 2D and 3D modes of interaction (Figure 7). For compounds **14, 15,** and **17,** the 2D and 3D modes of interactions with *E. coli* DNA gyrase B are depicted in Figure S26.

The docking analysis against PqsA indicated that the binding affinity of isolated compounds ranged from −9.3 to −6.3 kcal/mol compared with the docking score of ciprofloxacin (−7.2 kcal/mol). The highest docking score was observed with compound **16** (−9.3 kcal/mol), whereas the lowest binding score was seen with compound **15** (−6.3 kcal/mol). Compound **16** interacted with PqsA through five hydrogen bonds, while compound **15** interacted with PqsA through only one hydrogen bond. The value of binding affinity, which is not only determined by the number of bonds, is affected by various factors like the bond length and type of hydrogen bonds as discussed in the literature.[64,65] Compound **16**, the compound with good antibacterial activity against *P. aeruginosa* (11.70 ± 0.24 mm, Table 6), exhibited the highest binding score (−9.3 kcal/mol) with PqsA depicted in the form of 2D and 3D modes of interactions (Figure 8). The 2D and 3D modes of interaction of compounds **14**, **15**, and **17** against PqsA are shown in Figure S27. In conclusion, the in *silico* antibacterial study supported the in *vitro* antibacterial activities test and shows the potential of the isolated compounds as antibacterial agents.

The results of the docking analysis against PKM2 and human topoisomerase IIβ were compared with the results of the positive controls PKM2-IN-1 and etoposide (Table 9), respectively. The docking against PKM2 showed that the docking scores of isolated compounds ranged from −10.5 to −4.1 kcal/mol compared to the docking score of PKM2-IN-1 (−9.5 kcal/mol). The highest binding affinity (−9.6 kcal/mol) was shown by compound **16,** while the lowest (−4.1 kcal/mol) was seen with compound **14**. Compound **16,** with the highest binding affinity (−9.6 kcal/mol), interacted with PKM2 using six hydrogen bonds through Lys-311, 311, Gly-315, Asp-354, Tyr-390, and Leu-394 amino acid residues. In contrast, compound **14,** with the lowest binding affinity (−4.1 kcal/mol) interacted with PKM2 using only two hydrogen bonds through Asp-354 and Asn-350 amino acid residues. In another way, six hydrogen bonds were observed in the interaction between compound **17** and PKM2. However, the binding affinity of compound **17** was less than that of compound **16**. This condition might be related to factors such as the strength of the hydrogen bond and bond length.[64,65] The interaction of the compound with the highest binding affinity (compound **16**, −9.6 kcal/mol) is shown in 2D and 3D modes (Figure 9). For other compounds, their 2D and 3D modes of interaction with PKM2 are listed in Figure S28.

The docking against human topoisomerase IIβ displayed that the binding affinity of isolated compounds ranged from −5.1 to −2.7 kcal/mol, compared with the binding affinity of etoposide (−5.3 kcal/mol). The highest docking score (−5.1 kcal/mol) was observed with compound **16,** while the lowest docking score (−2.7 kcal/mol) was observed with compound **15**. Compound

https://doi.org/10.1021/acsomega.4c10788
ACS Omega 2025, 10, 9547−9562

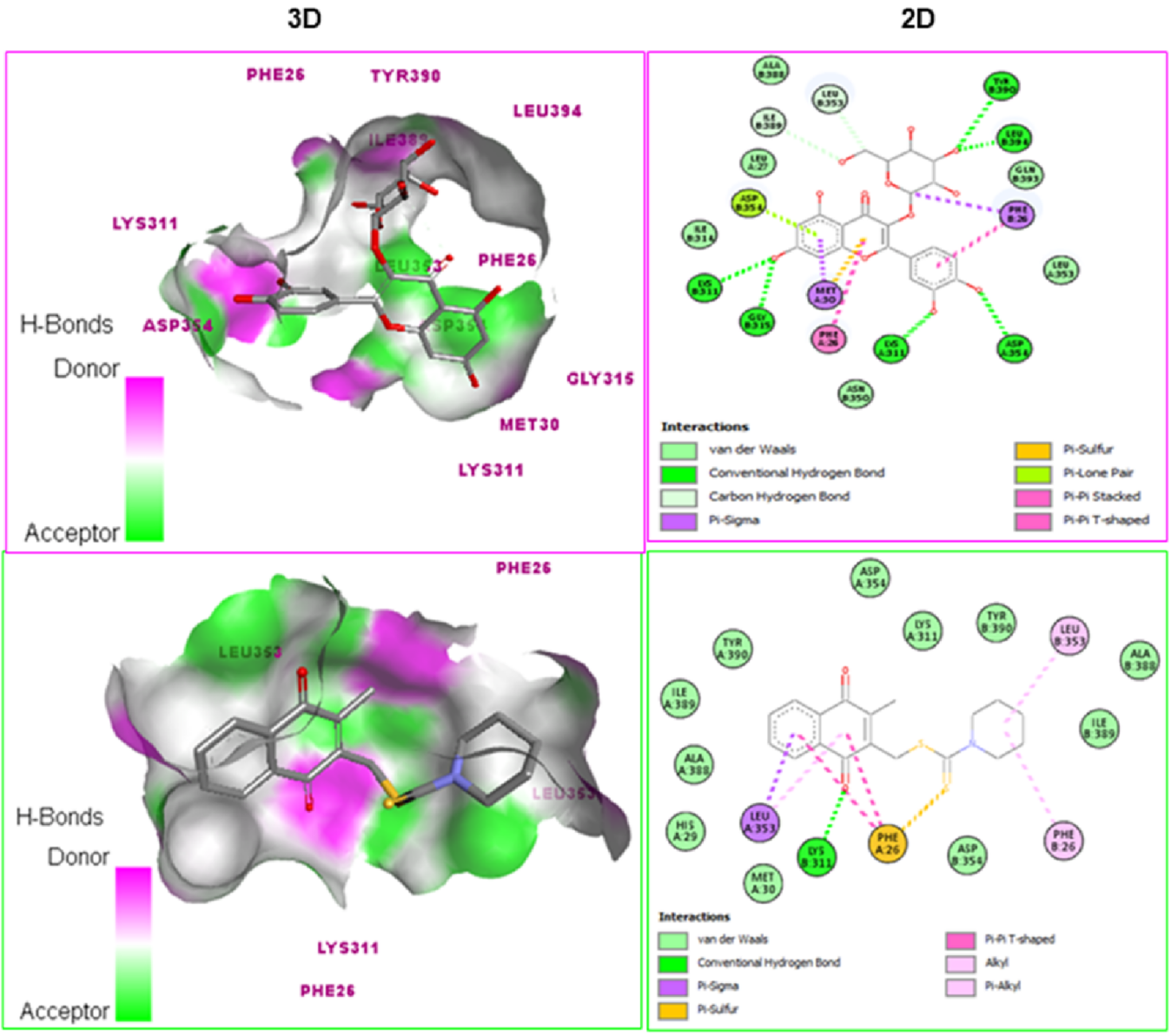

Figure 9. 3D and 2D binding interactions of compound **16** (top) and PKM2-IN-1 (bottom) with PKM2.

16, exhibiting the highest binding affinity, interacted with human topoisomerase IIβ using three hydrogen bonding interactions through Met-782, Gln-778, and Gly-776 amino acid residues, while compound **15**, with the lowest binding affinity, showed one hydrogen bonding interaction with human topoisomerase IIβ through Arg-503 amino residues. In addition, compound **16** demonstrated greater hydrophobic and electrostatic forces compared to compound **15**. The 2D and 3D modes of interaction of compound **16** are depicted in Figure 10. For the rest of the compounds, their 2D and 3D modes of interaction with human topoisomerase IIβ are displayed in Figure S29.

3.5. *In Silico* Pharmacokinetics and Toxicity of the Isolated Compounds. Table 10 shows the calculated drug-likeness properties of the isolated compounds using SwissADME following Lipinski's rule. As indicated, compounds **14** and **17** violate one of the rules stated in Lipinski's rule of five, whereas, similar to the standard anticancer drug, etoposide, compound **16** violates two rules among the rules described in Lipinski's rule of five. Unlike etoposide and the isolated compounds, positive controls ciprofloxacin and PKM2-IN-1 do not violate Lipinski's rule of five. As a rule, a drug that can be orally active has no more than one violation of the rule set in Lipinski's rule of five.[66] Therefore, except for compound **16**, the rest of the isolated compounds fulfill the rule stated in Lipinski's rule of five. Thus, compounds **14**, **15**, and **17** could be used as drugs orally because of their good solubility and permeability in the human bodies.

Table 11 presents the results of oral acute toxicity, organ toxicity, and toxicological end points calculated using the Pro Tox 3.0 online tool. Compounds **14** and **15** showed toxicity class 4, like the toxicity class of the standard antibacterial drug ciprofloxacin and the anticancer positive control PKM2-IN-1. Compounds **16** and **17** were predicted to be in toxicity class 5. Therefore, none of the isolated compounds were shown to be fatal if swallowed, as the predicted LD_{50} was greater than 50 mg/kg.[67]

Furthermore, compound **14** was predicted to affect the normal function of the heart, like some drugs claimed to cause cardiotoxicity through different mechanisms, and also affect the respiratory system through either of the multiple mechanisms

https://doi.org/10.1021/acsomega.4c10788
ACS Omega 2025, 10, 9547−9562

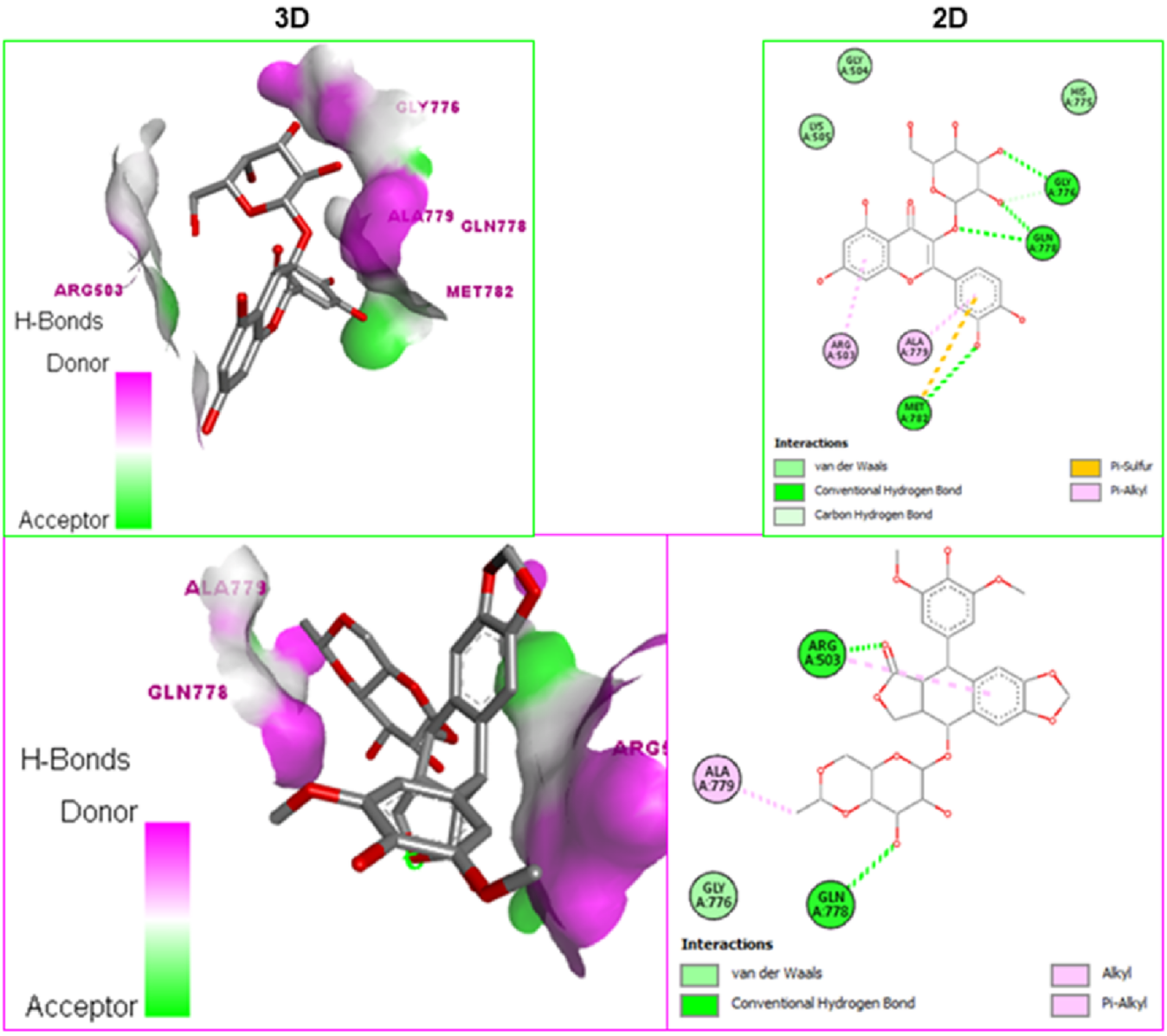

Figure 10. 3D and 2D binding interactions of compound **16** and etoposide against Human topoisomerase IIβ.

Table 10. Drug-likeness Predictions of Isolated Compounds Computed by SwissADME

comp.	molecular formula	MW/g/mol	NRB	NHA	NHD	TPSA (A^{o2})	log *P*(MLOGP ≤ 4.15)	log *S*/ESOL	Lipinski's rule of 5
14	$C_{30}H_{48}O_3$	456.7	1	3	2	57.5	5.82	−7.2	1
15	$C_6H_8O_3$	128.1	0	3	1	46.5	−0.11	−0.31	0
16	$C_{21}H_{20}O_{12}$	464.4	4	12	8	210.5	−2.59	−1.5	2
17	$C_{15}H_{18}O_9$	342.3	5	9	6	156.9	−1.63	−1.2	1
ciprofloxacin	$C_{17}H_{18}FN_3O_3$	331.3	3	5	2	74.6	1.28	−1.3	0
PKM2-IN-1	$C_{18}H_{19}NO_2S_2$	345.5	4	2	-	94.8	2.05	−4.13	0
etoposide	$C_{29}H_{32}O_{13}$	588.6	5	13	3	160.8	−0.14	−3.75	2

reported,[66,67] whereas compounds **16** and **17** were predicted to cause nephrotoxicity similar to drugs claimed to affect the normal function of the kidney.[68] Moreover, unlike compound **16**, compounds **14** and **17** are predicted as agents of immunotoxicity. The immune system serves as a guard to protect the body from disease-causing agents, such as fungi, parasites, bacteria, and viruses. This normal function can be affected by drugs that inhibit the immune system cells, including T and B lymphocytes.[69] In addition, compound **17**, like compound **15**, is predicted to affect the normal function of the blood−brain barrier (BBB). BBB is a blood vessel used to regulate the movement of ions, molecules, and cells between the blood and the brain.[70] Some drugs affect the normal function of the BBB; for example, increasing its permeability increases the influx of toxic materials to the brain.[71] In general, from these results, we conclude that compound **16** is less toxic than the other isolated compounds and the positive control.

https://doi.org/10.1021/acsomega.4c10788
ACS Omega 2025, 10, 9547−9562

Table 11. Toxicity Predictions of Isolated Compounds Calculated Using the Pro Tox II Online tool

comp.	LD_{50} (mg/kg)	toxicity class	organ toxicity	toxicological end points
14	2000	4	respiratory toxicity and cardiotoxicity	immunotoxicity
15	1890	4		BBB
16	5000	5	nephrotoxicity	
17	4000	5	nephrotoxicity	immunotoxicity and BBB
ciprofloxacin	2000	4	neurotoxicity, nephrotoxicity, and respiratory toxicity	mutagenicity and clinical toxicity
PKM2-IN-1	500	4	respiratory toxicity	BBB
etoposide	215	3	respiratory toxicity and cardiotoxicity	immunotoxicity

4. CONCLUSIONS

In this study, we report for the first time the identification of 13 compounds from the DCM/MeOH (1:1) extract of the leaves of *O. rochetiana* based on GC−MS spectral data. Additionally, four compounds, i.e., ursolic acid (**14**), 5,6-dihydro-4-methyl-(2*H*)-pyran-2-one (**15**), quercetin-3-*O*-(*β*-D-galactopyranoside) (**16**), and 4-*O*-*β*-D-glucopyranosylcaffeic acid (**17**), were isolated from the extract, and their structures were established using 1D and 2D NMR data. The antibacterial activities were evaluated against *S. aureus*, *S. pyogenes*, *E. coli*, and *P. aeruginosa*. The antioxidant activity was performed using the DPPH radical scavenging assay. The molecular docking was conducted against *E. coli* DNA gyrase B, PqsA, PKM2, and human topoisomerase II*β*. The drug-likeness and toxicity properties of the isolated compounds were predicted using SwissADME and Pro Tox 3.0 online tools, respectively. Based on the findings of this study, compound **14** was identified as a good antibacterial agent for *S. pyogenes*. Compound **16** was selected as a more effective antibacterial agent for both *E. coli* and *P. aeruginosa*. On the other hand, compound **17** was considered a better antibacterial agent for *S. aureus*. Therefore, compounds **14** and **17** exhibit strong antibacterial properties against Gram-positive bacteria, and compound **16** is a good antibacterial agent against Gram-negative bacteria. The antibacterial activity of compound **16** was validated using a molecular docking study against bacterial enzymes *E. coli* DNA gyrase B and PqsA for *E. coli*and *P. aeruginosa*bacteria, respectively. Furthermore, compound **16** can be considered a promising anticancer agent, as it effectively scavenges DPPH radicals and exhibits strong stabilization of the complex with the target enzymes PKM2 and human topoisomerase II*β*, both of which play crucial roles in the proliferation of cancer cells. Except for compound **16**, all isolated compounds were predicted to have good solubility and permeability in the human body. All isolated compounds are nonlethal, exhibit lower toxicity levels compared to the positive control used in this study, and are suitable for oral administration. These findings reinforce the traditional use of the plant as a remedy for various bacterial diseases. However, the synergetic effect of isolated compounds or using further isolation and characterization techniques for compounds found in smaller amounts can be the focus of the next study. In addition, *in vivo* studies are essential to assessing the biological and toxicological properties of the isolated compounds.

■ ASSOCIATED CONTENT

Data Availability Statement

The data recorded in this study are included in the manuscript and its Supporting Information.

Supporting Information

The Supporting Information is available free of charge at https://pubs.acs.org/doi/10.1021/acsomega.4c10788.

Total ion chromatogram (TIC) of combined fractions 4−17 (Figure S1); the ^{1}H, ^{13}C, DEPT-135, $^{1}H-^{13}C$ HSQC, $^{1}H-^{13}C$ HMBC, and $^{1}H-^{1}H$ COSY NMR spectral data of compounds **14**−**17** (Figures S2−S25); the 2D and 3D model interactions of compounds **14**−**17** against selected protein targets (Figures S26−S29); and TLC profiles of fractions and isolated compounds (Figure S30) (PDF)

■ AUTHOR INFORMATION

Corresponding Author

Yadessa Melaku − *Department of Applied Chemistry, Adama Science and Technology University, 1888 Adama, Oromia, Ethiopia;* orcid.org/0000-0003-2599-0517; Email: yadessa.melaku@astu.edu.et

Authors

Tolessa Duguma − *Department of Applied Chemistry, Adama Science and Technology University, 1888 Adama, Oromia, Ethiopia*

Daniel Rentsch − *Laboratory for Functional Polymers, Empa, Swiss Federal Laboratories for Materials Science and Technology, Duebendorf CH-8600, Switzerland;* orcid.org/0000-0002-9335-9527

Mo Hunsen − *Department of Chemistry, Kenyon College, Gambier, Ohio 43022, United States*

Taye B. Demissie − *Department of Chemistry, University of Botswana, Gaborone 00704, Botswana;* orcid.org/0000-0001-8735-4933

Nayang Kgakatsi − *Department of Chemistry, University of Botswana, Gaborone 00704, Botswana*

Complete contact information is available at: https://pubs.acs.org/10.1021/acsomega.4c10788

Author Contributions

T.D. planned the study, conducted the investigation, analyzed and interpreted the data, and wrote the original draft of the manuscript. Y.M. planned the study, supervised, analyzed and interpreted the data, and reviewed and edited the manuscript. D.R., M.H., T.B.D., and N.K. conducted an NMR analysis and reviewed and edited the manuscript.

Funding

The Institute of Pharmaceutical Science of Adama Science and Technology University provided funding for this study under grant ASTU/AS-R/001/2020.

Notes

The authors declare no competing financial interest.

■ ACKNOWLEDGMENTS

We are thankful to Urgessa Ensermu for conducting antibacterial activities and Kebede Shenkute for the GC−MS analysis.

REFERENCES

(1) POWO. *Plants of the world online. Facilitated by the Royal Botanic Gardens, Kew*. http://www.plantsoftheworldonline.org/ (accessed 2022−11−27).

(2) Tuasha, N.; Petros, B.; Asfaw, Z. Medicinal plants used by traditional healers to treat malignancies and other human ailments in Dalle District, Sidama Zone, Ethiopia. *J. Ethnobiol. Ethnomed.* **2018**, *14* (1), 15.

(3) Chekole, G. Ethnobotanical Study of medicinal plants used against human ailments in Gubalafto District, Northern Ethiopia. *J. Ethnobiol. Ethnomed.* **2017**, *13* (1), 55.

(4) Seble, W. Y.; Zemede, A.; Ensermu, K. Ethnobotanical study of medicinal plants used by local people in Menz Gera Midir District, North Shewa Zone, Amhara Regional State, Ethiopia. *J. Med. Plants Res.* **2018**, *12* (21), 296−314.

(5) Mulugeta, K. Diversity, knowledge and use of medicinal plants in Abay Chomen District, Horo Guduru Wollega Zone, Oromia Region of Ethiopia. *J. Med. Plants Res.* **2017**, *11* (31), 480−500.

(6) Nuro, G.; Tolossa, K.; Giday, M. Medicinal plants used by Oromo community in Kofale District, West-Arsi Zone, Oromia Regional State, Ethiopia. *J. Exp. Pharmacol.* **2024**, *2024* (16), 81−109.

(7) Woldeamanuel, M. M.; Geda, M. K.; Mohapatra, S.; Bastia, T. K.; Rath, P.; Panda, A. K. Ethnobotanical study of endemic and non-endemic medicinal plants used by indigenous people in environs of Gullele Botanical Garden Addis Ababa, Central Ethiopia: A major focus on Asteraceae family. *Front. Pharmacol.* **2022**, *13*, No. 1020097.

(8) Kefalew, A.; Asfaw, Z.; Kelbessa, E. Ethnobotany of medicinal plants in Ada'a District, East Shewa Zone of Oromia Regional State, Ethiopia. *J. Ethnobiol. Ethnomed.* **2015**, *11* (1), 25.

(9) Lulekal, E.; Asfaw, Z.; Kelbessa, E.; Van Damme, P. Ethno-medicinal study of plants used for human ailments in Ankober District, North Shewa Zone, Amhara Region, Ethiopia. *J. Ethnobiol. Ethnomed.* **2013**, *9* (1), 63.

(10) Tefera, B. N.; Kim, Y.-D. Ethnobotanical study of medicinal plants in the Hawassa Zuria District, Sidama Zone, Southern Ethiopia. *J. Ethnobiol. Ethnomed.* **2019**, *15* (25), 1−21.

(11) Teka, A.; Rondevaldova, J.; Asfaw, Z.; Demissew, S.; Van Damme, P.; Kokoska, L.; Vanhove, W. In vitro antimicrobial activity of plants used in traditional medicine in Gurage and Silti Zones, South Central Ethiopia. *BMC Complement. Altern. Med.* **2015**, *15* (1), 286.

(12) Omari, A.; Mulei, J.; Jeruto, P. Intrinsic biological activities of crude methanol extracts of *Olinia rochetiana* Penaeceae (Syn. O. Osambarensis Gilg) A. JUSS (Kabideleliet). *Eur. J. Biomed. Pharm. Sci.* **2013**, *2* (5), 83−89.

(13) Nigussie, G.; Erdedo, A.; Ashenafi, S. In vitro anti-bacterial activities of aqueous, ethanol and chloroform crude extracts of Olinia rochetiana and Vernonia myriantha. *J. Trop. Pharm. Chem.* **2020**, *5* (2), 98−110.

(14) Tadeg, H.; Mohammed, E.; Asres, K.; Gebre-Mariam, T. Antimicrobial activities of some selected traditional Ethiopian medicinal plants used in the treatment of skin disorders. *J. Ethnopharmacol.* **2005**, *100* (1−2), 168−175.

(15) Mekuriaw, E.; Mengistu, E.; Erdedo, A.; Mamo, H. In vitro antibacterial activity, preliminary phytochemical screening profile, and in vivo toxicity of seven traditional medicinal plants in Ethiopia. *J. Trad. Integrative Med.* **2022**, *6* (4), 398−414.

(16) Terefe, L.; Nardos, A.; Debella, A.; Dereje, B.; Arega, M.; Abebe, A.; Gemechu, W.; Woldekidan, S. Antidiarrheal activities of the methanol leaf extracts of Olinia rochetiana (Oliniaceae) against castor oil-induced diarrhea in mice. *J. Exp. Pharmacol.* **2023**, *15*, 485−495.

(17) Nahrstedt, A.; Rockenbach, J. Occurrence of the cyanogenic glucoside prunasin and corresponding mandelic acid amide glucoside in Olinia species (Oliniaceae). *Phytochemistry.* **1993**, *34* (2), 433−436.

(18) Dinku, W.; Choi, S. U.; Lee, S.-H.; Jung, Y.-S.; No, Z. S.; Dekebo, A. Antiproliferative effect of sterols from resin of Commiphora habessinica. *J. Pharm. Nutr. Sci.* **2019**, *9* (2), 71−80.

(19) Kim, S.; Chen, J.; Cheng, T.; Gindulyte, A.; He, J.; He, S.; Li, Q.; Shoemaker, B. A.; Thiessen, P. A.; Yu, B.; Zaslavsky, L.; Zhang, J.; Bolton, E. E. PubChem 2023 Update. *Nucleic Acids Res.* **2023**, *51* (D1), D1373−D1380.

(20) Hudzicki, J. *Kirby-Bauer disk diffusion susceptibility test protocol*. https://asm.org/getattachment/2594ce26-bd44-47f6-8287-0657aa9185ad/Kirby-Bauer-Disk-Diffusion-Susceptibility-Test-Protocol-pdf.pdf (accessed 2024−03−07).

(21) Grujic, S.; Radojevic, I.; Vasic, S.; Comic, L.; Topuzovic, M. Antimicrobial activity and some phytochemical analysis of two extracts Vinca minor L. *Kragujevac J. Sci.* **2014**, *36*, 145−154.

(22) Khlifi, D.; Hamdi, M.; Hayouni, A. El; Cazaux, S.; Souchard, J. P.; Couderc, F.; Bouajila, J. Global chemical composition and antioxidant and anti-tuberculosis activities of various extracts of Globularia alypum L. (Globulariaceae) leaves. *Molecules* **2011**, *16* (12), 10592−10603.

(23) Rizvi, S. M. D.; Shakil, S.; Haneef, M. A simple click by click protocol to perform docking: AutoDock 4.2 made easy for non-bioinformaticians. *EXCLI J.* **2013**, *12*, 831−857.

(24) BIOVA. *Dassault Systemes, discovery studio visualizer*. https://discover.3ds.com/discovery-studio-visualizer-download. (accessed 2024−03−07).

(25) Berman, H. M. The protein data bank. *Nucleic Acids Res.* **2000**, *28* (1), 235−242.

(26) Daina, A.; Michielin, O.; Zoete, V. SwissADME: A free web tool to evaluate pharmacokinetics, drug-likeness and Medicinal Chemistry friendliness of small molecules. *Sci. Rep.* **2017**, *7* (42717), 1−12.

(27) Banerjee, P.; Eckert, A. O.; Schrey, A. K.; Preissner, R. Protox-II: A Webserver for the prediction of toxicity of chemicals. *Nucleic Acids Res.* **2018**, *46* (W1), W257−W263.

(28) Gonzalez-Rivera, M. L.; Barragan-Galvez, J. C.; Gasca-Martínez, D.; Hidalgo-Figueroa, S.; Isiordia-Espinoza, M.; Alonso-Castro, A. J. In vivo neuropharmacological effects of neophytadiene. *Molecules.* **2023**, *28* (8), 3457.

(29) Selmy, A.; Hegazy, M.; El-Hela, A.; Saleh, A.; El-Hamouly, M. In vitro and in silico studies of neophytadiene; a diterpene isolated from Aeschynomene elaphroxylon (Guill. & Perr.) Taub. as apoptotic. *Egypt J. Chem.* **2023**, *66* (10), 149−161.

(30) Bhardwaj, M.; Sali, V. K.; Mani, S.; Vasanthi, H. R. Neophytadiene from Turbinaria ornata suppresses LPS-induced inflammatory response in RAW 264.7 macrophages and Sprague dawley rats. *Inflammation.* **2020**, *43* (3), 937−950.

(31) Ceyhan-Güvensen, N.; Keskin, D. Chemical content and antimicrobial properties of three different extracts of Mentha pulegium leaves from Mugla Region, Turkey. *J. Environ. Biol.* **2016**, *37* (6), 1341−1346.

(32) Luckanatinvong, V.; Mahatheeranont, S.; Siriphanich, J. Variation in the aromatic nature of Nam-Hom coconut depends on the presence and contents of 2-Acetyl-1-pyrroline. *Sci. Hortic.* **2018**, *233*, 277−282.

(33) Priya, N. P.; Jones, R. S. Larvicidal activity and GC-MS analysis of Piper longum L. leaf extract fraction against human vector mosquitoes (Diptera: Culicidae). *Int. J. Mosq. Res.* **2021**, *8* (4), 31−37.

(34) Bhart, D.; Arif, M.; Ahmad, M.; Khan, A. A.; Usmani, A.; Ajmal, M.; Siddiqui, M. A. Phytochemical and antioxidant characterization of ethanolic extract of Zea Mays. *Pak. Heart J.* **2023**, *56* (02), 1242−1247.

(35) Saeed, N. M.; El-Demerdash, E.; Abdel-Rahman, H. M.; Algandaby, M. M.; Al-Abbasi, F. A.; Abdel-Naim, A. B. Anti-inflammatory activity of methyl palmitate and ethyl palmitate in different experimental rat models. *Toxicol. Appl. Pharmacol.* **2012**, *264* (1), 84−93.

(36) Deora, A.; Hatano, E.; Tahara, S.; Hashidoko, Y. Inhibitory effects of furanone metabolites of a Rhizobacterium, Pseudomonas jessenii, on phytopathogenic phanomyces cochlioides and Pythium aphanidermatum. *Plant Pathol.* **2010**, *59* (1), 84−99.

(37) Sang, Y.; Liu, J.; Shi, L.; Wang, X.; Xin, Y.; Hao, Y.; Bai, L. Study on gas chromatographic fingerprint of essential oil from Stellera chamaejasme flowers and its repellent activities against three stored product insects. *Molecules* **2021**, *26* (21), 6438.

(38) Khan, M.; Yusufzai, S.; Kaun, L.; Shah, M.; Idris, R. chemical composition and antioxidant activity of essential oil of leaves and

https://doi.org/10.1021/acsomega.4c10788
ACS Omega 2025, 10, 9547−9562

flowers of Alternanthera sessilis red from Sabah. *J. Appl. Pharm. Sci.* **2016**, 157−161.
(39) Shobi, T. M.; Viswanathan, M. B. G. Antibacterial activity of dibutyl phthalate isolated from Begonia malabarica. *J. Appl. Biotechnol. Bioeng.* **2018**, *5* (2), 97.
(40) Yasmin, F.; Nazli, Z.-H.; Shafiq, N.; Aslam, M.; Bin Jardan, Y. A.; Nafidi, H.-A.; Bourhia, M. Plant-based bioactive phthalates derived from Hibiscus Rosa-sinensis: As in vitro and in silico enzyme inhibition. *ACS Omega.* **2023**, *8* (36), 32677−32689.
(41) Estella, O. U.; Sangwan, P. L. Isolation and characterization of ursolic acid, apigenin, and luteolin from leaves of Starchytarpheta jamaicensis (L) Vahl (Verbennaceae) from tropical forest of Eastern Nigeria. *World J. Pharm. Res.* **2020**, *9* (9), 11−21.
(42) Seebacher, W.; Simic, N.; Weis, R.; Saf, R.; Kunert, O. Complete assignments of ^{1}H and ^{13}C NMR resonances of oleanolic acid, 18α-oleanolic acid, ursolic acid and their 11-oxo derivatives. *Magn. Reson. Chem.* **2003**, *41* (8), 636−638.
(43) do Nascimento, P. G. G.; Lemos, T. L. G.; Bizerra, A. M. C.; Arriaga, Â. M. C.; Ferreira, D. A.; Santiago, G. M. P.; Braz-Filho, R.; Costa, J. G. M. Antibacterial and antioxidant activities of ursolic acid and derivatives. *Molecules.* **2014**, *19* (1), 1317−1327.
(44) Prasad, S.; Yadav, V. R.; Sung, B.; Gupta, S. C.; Tyagi, A. K.; Aggarwal, B. B. Ursolic acid inhibits the growth of human pancreatic cancer and enhances the antitumor potential of gemcitabine in an orthotopic mouse model through suppression of the inflammatory microenvironment. *Oncotarget.* **2016**, *7* (11), 13182−13196.
(45) Tang, S.; Fang, C.; Liu, Y.; Tang, L.; Xu, Y. Anti-obesity and anti-diabetic effect of ursolic acid against Streptozotocin/high fat induced obese in diabetic rats. *J. Oleo. Sci.* **2022**, *71* (2), No. ess21258.
(46) Akihisa, T.; Ogihara, J.; Kato, J.; Yasukawa, K.; Ukiya, M.; Yamanouchi, S.; Oishi, K. Inhibitory effects of triterpenoids and sterols on human immunodeficiency virus-1 reverse transcriptase. *Lipids.* **2001**, *36* (5), 507−512.
(47) Deyou, T.; Woo, J.-H.; Choi, J.-H.; Jang, Y. P. A new natural product from the leaves of Olinia usambarensis and evaluation of its constituents for cytotoxicity against human ovarian cancer cells. *S. Afr. J. Bot.* **2017**, *113*, 182−185.
(48) Jiang, L.; Numonov, S.; Bobakulov, K.; Qureshi, M.; Zhao, H.; Aisa, H. Phytochemical profiling and evaluation of pharmacological activities of Hypericum scabrum L. *Molecules.* **2015**, *20* (6), 11257−11271.
(49) Nyandat, E.; Rwekika, E.; Galeffi, C.; Palazzino, G.; Nicoletti, M. Olinioside, 5-(4′-O-β-d-Glucopyranosyl)-Caffeoyloxy-5,6- Dihydro-4-Methyl-(2H)-Pyran-2-One from Olinia usambarensis. *Phytochemistry.* **1993**, *33* (6), 1493−1496.
(50) Park, J. Y.; Han, X.; Piao, M. J.; Oh, M. C.; Fernando, P. M. D. J.; Kang, K. A.; Ryu, Y. S.; Jung, U.; Kim, I. G.; Hyun, J. W. Hyperoside induces endogenous antioxidant system to alleviate oxidative stress. *J. Cancer. Prev.* **2016**, *21* (1), 41−47.
(51) Tagrida, M.; Palamae, S.; Saetang, J.; Ma, L.; Hong, H.; Benjakul, S. Comparative study of quercetin and hyperoside: Antimicrobial potential towards food spoilage bacteria, mode of action and molecular docking. *Foods* **2023**, *12* (22), 4051.
(52) Feng, Y.; Qin, G.; Chang, S.; Jing, Z.; Zhang, Y.; Wang, Y. Antitumor effect of hyperoside loaded in charge reversed and mitochondria-targeted liposomes. *Int. J. Nanomedicine.* **2021**, *16*, 3073−3089.
(53) Zhang, Y.; Wang, M.; Dong, H.; Yu, X.; Zhang, J. Anti-hypoglycemic and hepatocyte-protective effects of hyperoside from Zanthoxylum bungeanum leaves in mice with high-carbohydrate/high-fat diet and alloxan-induced diabetes. *Int. J. Mol. Med.* **2017**, *41* (1), 77−86.
(54) Jin, X.; Yan, E.; Wang, H.; Sui, H.; Liu, Z.; Gao, W.; Jin, Y. Hyperoside exerts anti-inflammatory and anti-arthritic effects in LPS-stimulated human fibroblast-like synoviocytes *in vitro* and in mice with collagen-induced arthritis. *Acta. Pharmacol. Sin* **2016**, *37* (5), 674−686.
(55) Li, S.; Zhang, Z.; Cain, A.; Wang, B.; Long, M.; Taylor, J. Antifungal Activity of Camptothecin, Trifolin, and hyperoside isolated from Camptotheca acuminata. *J. Agric. Food Chem.* **2005**, *53* (1), 32−37.
(56) Nofrizal; Putra, D. P.; Arbain, D. Antioxidant and Antibacterial Constituents from Two Sumatran Ferns,Trichomanes Javanicum and Oleandra Pistillaris. *Nat. Prod Commun.* **2017**, *12* (8), 1934578 × 1701200.
(57) Zhang, L.-J.; Huang, H.-T.; Huang, S.-Y.; Lin, Z.-H.; Shen, C.-C.; Tsai, W.-J.; Kuo, Y.-H. Antioxidant and anti-inflammatory phenolic glycosides from Clematis Tashiroi. *J. Nat. Prod.* **2015**, *78* (7), 1586−1592.
(58) Gil, M. I.; Tomás-Barberán, F. A.; Hess-Pierce, B.; Holcroft, D. M.; Kader, A. A. Antioxidant activity of pomegranate juice and its relationship with phenolic composition and processing. *J. Agric. Food Chem.* **2000**, *48* (10), 4581−4589.
(59) Costenaro, L.; Grossmann, J. G.; Ebel, C.; Maxwell, A. Modular structure of the full-length DNA gyrase B subunit revealed by small-angle x-ray scattering. *Structure.* **2007**, *15* (3), 329−339.
(60) Coleman, J. P.; Hudson, L. L.; McKnight, S. L.; Farrow, J. M.; Calfee, M. W.; Lindsey, C. A.; Pesci, E. C. *Pseudomonas Aeruginosa* PqsA is an anthranilate-coenzyme A ligase. *J. Bacteriol.* **2008**, *190* (4), 1247−1255.
(61) Mazurek, S. Pyruvate Kinase Type M2: A Key regulator of the metabolic budget system in tumor cells. *Int. J. Biochem. Cell Biol.* **2011**, *43* (7), 969−980.
(62) Zahra, K.; Dey, T.; Ashish; Mishra, S. P.; Pandey, U. Pyruvate kinase M2 and cancer: The role of PKM2 in promoting tumorigenesis. *Front. Oncol.* **2020**, *10*. .
(63) Wu, C.-C.; Li, T.-K.; Farh, L.; Lin, L.-Y.; Lin, T.-S.; Yu, Y.-J.; Yen, T.-J.; Chiang, C.-W.; Chan, N.-L. Structural basis of type II topoisomerase inhibition by the anticancer drug etoposide. *Science. (1979)* **2011**, *333* (6041), 459−462.
(64) Özen, A. S.; De Proft, F.; Aviyente, V.; Geerlings, P. Interpretation of hydrogen bonding in the weak and strong regions using conceptual DFT descriptors. *J. Phys. Chem. A* **2006**, *110* (17), 5860−5868.
(65) Owoloye, A. J.; Ligali, F. C.; Enejoh, O. A.; Musa, A. Z.; Aina, O.; Idowu, E. T.; Oyebola, K. M. Molecular docking, simulation and binding free energy analysis of small molecules as PfHT1 Inhibitors. *PLoS One.* **2022**, *17* (8), No. e0268269.
(66) Valiyaveettil, D.; Joseph, D.; Malik, M. Cardiotoxicity in breast cancer treatment: causes and mitigation. *Cancer Treat. Res. Commun.* **2023**, *37*, No. 100760.
(67) Matsuno, O. Drug-induced interstitial lung disease: Mechanisms and best diagnostic approaches. *Respir. Res.* **2012**, *13* (1), 39.
(68) Kim, S.-Y.; Moon, A.-R. Drug-induced nephrotoxicity and its biomarkers. *Biomol. Ther. (Seoul).* **2012**, *20* (3), 268−272.
(69) Bou Zerdan, M.; Moussa, S.; Atoui, A.; Assi, H. I. Mechanisms of immunotoxicity: stressors and evaluators. *Int. J. Mol. Sci.* **2021**, *22* (15), 8242.
(70) Daneman, R.; Prat, A. The blood-brain barrier. *Cold Spring Harb. Perspect. Biol.* **2015**, *7* (1), No. a020412.
(71) Pimentel, E.; Sivalingam, K.; Doke, M.; Samikkannu, T. Effects of drugs of abuse on the blood-brain barrier: A brief overview. *Front. Neurosci.* **2020**, *14*, 513.

https://doi.org/10.1021/acsomega.4c10788
ACS Omega 2025, 10, 9547−9562